Hydrological variations of the intermediate water masses of the western Mediterranean Sea during the past 20 ka inferred from neodymium isotopic composition in foraminifera and cold-water corals

Quentin Dubois-Dauphin[1], Paolo Montagna[2,3], Giuseppe Siani[1], Eric Douville[4], Claudia Wienberg[5], Dierk Hebbeln[5], Zhifei Liu[6], Nejib Kallel[7], Arnaud Dapoigny[4], Marie Revel[8], Edwige Pons-Branchu[4], Marco Taviani[2,9], Christophe Colin[1]*

[1]Laboratoire Geosciences Paris-Sud (GEOPS), Université de Paris Sud, Université Paris-Saclay, 91405 Orsay, France.
[2]ISMAR-CNR, via Gobetti 101, 40129 Bologna, Italy.
[3]Lamont-Doherty Earth Observatory, Columbia University, 61 Route 9W, Palisades, NY 10964, USA
[4]Laboratoire des Sciences du Climat et de l'Environnement, LSCE/IPSL, CEA-CNRS-UVSQ, Université Paris-Saclay, F-91191 Gif-sur-Yvette, France.
[5]MARUM-Center for Marine Environmental Sciences, University of Bremen, Leobener Strasse, 28359 Bremen, Germany.
[6]State Key Laboratory of Marine Geology, Tongji University, Shanghai 200092, China.
[7]Laboratoire Georessources, Matériaux, Environnements et Changements Globaux, LR13ES23, Faculté des Sciences de Sfax, Université de Sfax, BP1171, 3000 Sfax, Tunisia.
[8]Geoazur, UNS, IRD, OCA, CNRS, 250 rue Albert Einstein, 06500 Valbonne, France
[9]Biology Department, Woods Hole Oceanographic Institution, 266 Woods Hole Road, Woods Hole, MA 02543, USA.

Correspondence to: Christophe Colin (christophe.colin@u-psud.fr)

Abstract. We present the neodymium isotopic composition (εNd) of mixed planktonic foraminifera species from a sediment core collected at 622 m water depth in the Balearic Sea, as well as εNd of scleractinian cold-water corals (CWC; *Madrepora oculata, Lophelia pertusa*) retrieved at 280-414 m water depth in the Alboran Sea and the south Sardinian continental margin. The aim is to constrain hydrological variations at intermediate depths in the western Mediterranean Sea during the last 20 kyr. Planktonic (*Globigerina bulloides*) and benthic (*Cibicidoides pachyderma*) foraminifera were also analyzed for stable oxygen (δ^{18}O) and carbon (δ^{13}C) isotopes. The foraminiferal and coral εNd values from the Balearic and Alboran Sea are comparable over the last ~13 kyr, with mean values of -8.94±0.26 (1σ; n=24) and -8.91±0.18 (1σ; n=25), respectively. Before 13 ka BP, the foraminiferal εNd values are slightly lower (-9.28±0.15) and tend to reflect a higher mixing between intermediate and deep waters, which is characterized by more unradiogenic εNd values. The slight εNd increase after 13 ka BP is associated to a decoupling in the benthic foraminiferal δ^{13}C composition between intermediate and deeper depths, which started at ~16 ka BP. This suggests an earlier stratification of the water masses and a subsequent reduced contribution of unradiogenic εNd from deep waters. The CWC from the Sardinia Channel show a much larger scattering of εNd values, from -8.66±0.30 to -5.99±0.50, and a lower average (-7.31±0.73; n=19) compared to the CWC and foraminifera from the Alboran and Balearic Sea, indicative of intermediate waters sourced from the Levantine basin. At the time of sapropel S1 deposition (10.2 to 6.4 ka), the εNd values of the Sardinian CWC become more unradiogenic (-8.38±0.47; n=3 at ~8.7 ka BP), suggesting a significant contribution of intermediate waters originated from the western basin. Accordingly, we propose that western

47 Mediterranean intermediate waters replaced the Levantine Intermediate Water (LIW), which was strongly

48 reduced during the mid-sapropel (~8.7 ka BP). This observation supports a notable change of Mediterranean

49 circulation pattern centered on sapropel S1 that needs further investigations to be confirmed.

50

51 **1. Introduction**

52 The Mediterranean Sea is a mid-latitude semi-enclosed basin, characterized by evaporation exceeding

53 precipitation and river runoff, where the inflow of fresh and relatively warm surface Atlantic water is

54 transformed into saltier and cooler (i.e. denser) intermediate and deep waters. Several studies have demonstrated

55 that the Mediterranean thermohaline circulation was highly sensitive to both the rapid climatic changes

56 propagated into the basin from high latitudes of the Northern Hemisphere (Cacho et al., 1999, 2000, 2002;

57 Moreno et al., 2002, 2005; Paterne et al., 1999; Martrat et al., 2004; Sierro et al., 2005; Frigola et al., 2007,

58 2008) and orbitally-forced modifications of the eastern Mediterranean freshwater budget mainly driven by

59 monsoonal river runoff from the south (Rohling et al., 2002; 2004; Bahr et al., 2015). A link between the

60 intensification of the Mediterranean Outflow Water (MOW) and the intensity of the Atlantic Meridional

61 Overturning Circulation (AMOC) was proposed (Cacho et al., 1999, 2000, 2001; Bigg and Wadley, 2001; Sierro

62 et al., 2005; Voelker et al., 2006) and recently supported by new geochemical data in sediments of the Gulf of

63 Cádiz (Bahr et al., 2015). In particular, it has been suggested that the intensity of the MOW and, more generally,

64 the variations of the thermohaline circulation of the Mediterranean Sea could play a significant role in triggering

65 a switch from a weakened to an enhanced state of the AMOC through the injection of saline Mediterranean

66 waters in the intermediate North Atlantic at times of weak AMOC (Rogerson et al., 2006; Voelker et al., 2006;

67 Khélifi et al., 2009). The Mediterranean intermediate waters, notably the Levantine Intermediate Water (LIW),

68 which represent today up to 80 % in volume of the MOW (Kinder and Parilla, 1987) are considered an important

69 driver of MOW-derived salt into the North Atlantic. Furthermore, the LIW also plays a key role in controlling

70 the deep-sea ventilation of the Mediterranean basin, being strongly involved in the formation of deep waters in

71 the Aegean Sea, Adriatic Sea, Tyrrhenian Sea and Gulf of Lions (Millot and Taupier-Letage, 2005). It is

72 hypothesized that a reduction of intermediate and deep-water formation as a consequence of surface hydrological

73 changes in the eastern Mediterranean basin acted as a precondition for the sapropel S1 deposition by limiting the

74 oxygen supply to the bottom waters (De Lange et al., 2008; Rohling et al., 2015; Tachikawa et al., 2015).

75 Therefore, it is crucial to gain a more complete understanding of the variability of the Mediterranean

76 intermediate circulation in the past and its impact on the MOW outflow and, in general, on the Mediterranean

77 thermohaline circulation.

78 Previous studies have mainly focused on the glacial variability of the deep-water circulation in the western

79 Mediterranean basin (Cacho et al., 2000, 2006; Sierro et al., 2005; Frigola et al., 2007, 2008). During the Last

80 Glacial Maximum (LGM), strong deep-water convection took place in the Gulf of Lions, producing cold, well-

81 ventilated western Mediterranean Deep Water (WMDW) (Cacho et al., 2000, 2006; Sierro et al., 2005), while

82 the MOW flowed at greater depth in the Gulf of Cádiz (Rogerson et al., 2005; Schönfeld and Zahn, 2000). With

83 the onset of the Termination 1 (T1) at about 15 ka, the WMDW production declined until the transition to the

84 Holocene due to the rising sea level, with a relatively weak mode during the Heinrich Stadial 1 (HS1) and the

85 Younger Dryas (YD) (Sierro et al., 2005; Frigola et al., 2008), that led to the deposition of the Organic Rich

86 Layer 1 (ORL1; 14.5-8.2 ka BP; Cacho et al., 2002).

87   Because of the disappearance during the Early Holocene of specific epibenthic foraminiferal species, such as
88   *Cibicidoides* spp., which are commonly used for paleohydrological reconstructions, information about the
89   Holocene variability of the deep-water circulation in the western Mediterranean are relatively scarce and are
90   mainly based on grain size analysis and sediment geochemistry (e.g. Frigola et al., 2007). These authors have
91   identified four distinct phases representing different deep-water overturning conditions in the western
92   Mediterranean basin during the Holocene, as well as centennial- to millennial-scale abrupt events of overturning
93   reinforcement.

94   Faunal and stable isotope records from benthic foraminifera located at intermediate depths in the eastern basin
95   reveal uninterrupted well-ventilated LIW during the last glacial period and deglaciation (Kuhnt et al., 2008;
96   Schmiedl et al., 2010). Similarly, a grain-size record obtained from a sediment core collected within the LIW
97   depth range (~500 m water depth) at the east Corsica margin also documents enhanced bottom currents during
98   the glacial period and for specific time intervals during the deglaciation, such as HS1 and YD (Toucanne et al.,
99   2012). The Early Holocene is characterized by a collapse of the LIW (Kuhnt et al., 2008; Schmiedl et al., 2010;
100 Toucanne et al., 2012) synchronous with the sapropel S1 deposition (10.2 – 6.4 cal ka BP; Mercone et al., 2000).
101 Proxies for deep-water conditions reveal the occurrence of episodes of deep-water overturning reinforcement in
102 the eastern Mediterranean basin at 8.2 ka BP (Rohling et al., 1997, 2015; Kuhnt et al., 2007; Abu-Zied et al.,
103 2008, Siani et al., 2013; Tachikawa et al; 2015), responsible for the interruption of the sapropel S1 in the eastern
104 Mediterranean basin (Mercone et al., 2001; Rohling et al., 2015).

105 Additional insights into Mediterranean circulation changes may be obtained using radiogenic isotopes, such as
106 neodymium, that represent reliable tracers for constraining water-mass mixing and sources (Goldstein and
107 Hemming, 2003, and references therein). It has recently been shown that the neodymium (Nd) isotopic
108 composition, expressed as εNd = ([(^{143}Nd/^{144}Nd)$_{sample}$ /(^{143}Nd/^{144}Nd)$_{CHUR}$] − 1) x 10000 (CHUR: Chondritic
109 Uniform Reservoir [Jacobsen and Wasserburg , 1980]) of living and fossil scleractinian CWC faithfully traces
110 intermediate and deep-water mass provenance and mixing of the ocean (e.g. van de Flierdt et al., 2010; Colin et
111 al., 2010; López Correa et al., 2012; Monterro-Serrano et al., 2011, 2013; Copard et al., 2012). Differently from
112 the CWC, the εNd composition of fossil planktonic foraminifera is not related to the ambient seawater at
113 calcification depths but reflects the bottom and/or pore water εNd, due to the presence of authigenic Fe-Mn
114 coatings precipitated on their carbonate shell (Roberts et al., 2010; Elmore et al., 2011; Piotrowski et al., 2012;
115 Tachikawa et al., 2014; Wu et al., 2015). Therefore, the εNd composition of planktonic foraminiferal tests can be
116 used as a useful tracer of deep-water circulation changes in the past, although the effect of pore water on
117 foraminiferal εNd values could potentially complicate the interpretation (Tachikawa et al., 2014).

118 In the Mediterranean Sea, modern seawater εNd values display a large range from ~-11 to ~-5, and a clear
119 vertical and longitudinal gradient, with more radiogenic values encountered in the eastern basin and typically at
120 intermediate and deeper depths (Spivack and Wasserburg 1988; Henry et al., 1994; Tachikawa et al., 2004;
121 Vance et al., 2004). Considering this large εNd contrast, εNd recorded in fossil CWC and planktonic
122 foraminifera from the Mediterranean offers great potential to trace intermediate and deep-water mass exchange
123 between the two basins, especially during periods devoid of key epibenthic foraminifera, such as the sapropel S1
124 or ORL1 events.

125 Here, the εNd of planktonic foraminifera from a sediment core collected in the Balearic Sea and CWC samples
126 from the Alboran Sea and the Sardinia Channel was investigated to establish past changes of the seawater εNd at

intermediate depths and constrain hydrological variations of the LIW during the last ~20 kyr. The εNd values have been combined with stable oxygen (δ^{18}O) and carbon (δ^{13}C) isotope measurements of benthic (*Cibicidoides pachyderma*) and planktonic (*Globigerina bulloides*) foraminifera and sea-surface temperature estimates by modern analogue technique (MAT). Results reveal significant εNd variations at intermediate depths in the western basin interpreted as a drastic reduction of the hydrological exchanges between the western and eastern Mediterranean Sea and the subsequent higher proportion of intermediate water produced in the Gulf of Lions during the time interval corresponding to the sapropel S1 deposition.

2. Seawater εNd distribution in the Mediterranean Sea

The Atlantic Water (AW) enters the Mediterranean Sea as surface inflow through the Strait of Gibraltar with an unradiogenic εNd signature of ~-9.7 in the strait (Tachikawa et al., 2004) and ~-10.4 in the Alboran Sea (Tachikawa et al., 2004, Spivack and Wasserburg, 1988) for depths shallower than 50 m. During its eastward flowing, AW mixes with upwelled Mediterranean Intermediate Water forming the Modified Atlantic Water (MAW) that spreads within the basin (Millot and Taupier-Letage, 2005) (Fig.1). The surface water εNd values (shallower than 50 m) range from -9.8 to -8.8 in the western Mediterranean basin (Henry et al., 1994; Montagna, pers. comm., 2016) and -9.3 to -4.2 in the eastern basin, with seawater off the Nile delta showing the most radiogenic values (Tackikawa et al., 2004; Vance et al., 2004; Montagna, pers. comm., 2016). The surface waters in the eastern Mediterranean basin become denser due to strong mixing and evaporation caused by cold and dry air masses flowing over the Cyprus-Rhodes area in winter, and eventually sink leading to the formation of LIW (Ovchinnikov, 1984; Lascaratos et al., 1993, 1998; Malanotte-Rizzoli et al., 1999; Pinardi and Masetti, 2000). The LIW spreads throughout the entire Mediterranean basin at depths between ~150-200 m and ~600-700 m, and is characterized by more radiogenic εNd values ranging from -7.9 to -4.8 (average value ± 1σ: -6.6 ± 1) in the eastern basin and from -10.4 to -7.58 (-8.7 ± 0.9) in the western basin (Henry et al., 1994; Tachikawa et al., 2004; Vance et al., 2004; Montagna, pers. comm., 2016). The LIW acquires its εNd signature mainly from the partial dissolution of Nile River particles (Tachikawa et al., 2004), which have an average isotopic composition of -3.25 (Weldeab et al., 2002), and the mixing along its path with overlying and underlying water masses with different εNd signatures. The LIW finally enters the Atlantic Ocean at intermediate depths through the Strait of Gibraltar with an average εNd value of -9.2 ± 0.2 (Tachikawa et al., 2004; Montagna, pers. comm., 2016).

The WMDW is formed in the Gulf of Lions due to winter cooling and evaporation followed by mixing between the relative fresh surface water and the saline LIW and spreads into the Balearic basin and Tyrrhenian Sea between ~2000 m and 3000 m (Millot, 1999; Schroeder et al., 2013) (Fig. 1). The WMDW is characterized by an average εNd value of -9.4 ± 0.9 (Henry et al., 1994; Tachikawa et al., 2004; Montagna, pers. comm., 2016). Between the WDMW and the LIW (from ~700 to 2000 m), the Tyrrhenian Deep Water (TDW) has been found (Millot et al., 2006), which is produced by the mixing between WMDW and Eastern Mediterranean Deep Water (EMDW) that cascades in the Tyrrhenian Sea after entering from the Strait of Sicily (Millot, 1999, 2009; Astraldi et al., 2001). The TDW has an average εNd value of -8.1 ± 0.5 (Montagna, pers. comm., 2016).

3. Material and methods

3.1. Cold-water coral and foraminifera samples

167 Forty-four CWC samples belonging to the species *Lophelia pertusa* and *Madrepora oculata* collected from the
168 Alboran Sea and the Sardinia Channel were selected for this study (Fig. 1). Nineteen fragments were collected at
169 various core depths from a coral-bearing sediment core (RECORD 23; 38°42.18' N; 08°54.75' E; Fig. 1)
170 retrieved from 414 m water depth in the "Sardinian Cold-Water Coral Province" (Taviani et al., 2015) during the
171 R/V Urania cruise "RECORD" in 2013. The core contains well-preserved fragments of *M. oculata* and *L.*
172 *pertusa* embedded in a brownish muddy to silty carbonate-rich sediment. The Sardinian CWC samples were
173 used for U-series dating and Nd isotopic composition measurements. For the southern Alboran Sea, twenty-five
174 CWC samples were collected at water depths between 280 and 442 m in the "eastern Melilla Coral Province"
175 (Fig. 1) during the R/V Poseidon cruise "POS-385" in 2009 (Hebbeln et al. 2009). Eleven samples were
176 collected at the surface of two coral mounds (New Mound and Horse Mound) and three coral ridges (Brittlestar
177 ridges I, II and III), using a box corer and a remotely operated vehicle (ROV). In addition, fourteen CWC
178 samples were collected from various core depths of three coral-bearing sediment cores (GeoB13728, 13729 and
179 13730) retrieved from the Brittlestar ridge I. Details on the location of surface samples and cores collected in the
180 southern Alboran Sea and details on the radiocarbon ages obtained from these coral samples are reported in Fink
181 et al. (2013). Like the CWC sample set from the Sardinia Channel, the dated Alboran CWC samples were also
182 used for further Nd isotopic composition analyses in this study.
183 In addition, a deep-sea sediment core (barren of any CWC fragments) was recovered southwest of the Balearic
184 Sea at 622 m water depth during the R/V Le Suroît cruise "PALEOCINAT II" in 1992 (SU92-33; 35°25.38' N;
185 0°33.86' E; Fig. 1). The core unit, which consists of 2.1 m of grey to brown carbonaceous clays, was sub-
186 sampled continuously at 5-10 cm intervals for a total number of 24 samples used for $\delta^{18}O$, $\delta^{13}C$ and ϵNd
187 analyzes.
188
189 ***3.2. Analytical procedures on cold-water coral samples***
190   *3.2.1. U/Th dating*
191 The nineteen CWC samples collected from the sediment core RECORD 23 (Sardinia Channel) were analysed for
192 uranium and thorium isotopes to obtain absolute dating using a Thermo Scientific™ Neptune^{Plus} MC-ICPMS
193 installed at the Laboratoire des Sciences du Climat et de l'Environnement (LSCE, Gif-sur-Yvette, France). Prior
194 to analysis, the samples were carefully cleaned using a small diamond blade to remove any visible contamination
195 and sediment-filled cavities. The fragments were examined under a binocular microscope to ensure against the
196 presence of bioeroded zones and finally crushed into a coarse-grained powder with an agate mortar and pestle.
197 The powders (~60-100 mg) were transferred to acid cleaned Teflon beakers, ultrasonicated in MilliQ water,
198 leached with 0.1N HCl for ~ 15 s and finally rinsed twice with MilliQ water. The physically and chemically
199 cleaned samples were dissolved in 3-4 ml dilute HCl (~10%) and mixed with an internal triple spike with known
200 concentrations of ^{229}Th, ^{233}U and ^{236}U, calibrated against a Harwell Uraninite solution (HU-1) assumed to be at
201 secular equilibrium. The solutions were evaporated to dryness at 70°C, redissolved in 0.6 ml 3N HNO_3 and then
202 loaded into 500 µl columns packed with Eichrom UTEVA resin to isolate uranium and thorium from the other
203 major and trace elements of the carbonate matrix. The U and Th separation and purification followed a
204 procedure slightly modified from Douville et al. (2010). The U and Th isotopes were determined following the
205 protocol recently revisited at LSCE (Pons-Branchu et al., 2014). The $^{230}Th/U$ ages were calculated from
206 measured atomic ratios through iterative age estimation (Ludwig and Titterington, 1994), using the ^{230}Th, ^{234}U

207 and ^{238}U decay constants of Cheng et al. (2013) and Jaffey et al. (1971). Due to the low ^{232}Th concentration (< 1
208 ng/g; see Table 1), no correction was applied for the non-radiogenic ^{230}Th fraction.

209

210   *3.2.2 Nd isotopic composition analyses on cold-water coral fragments*
211 Sub-samples of the CWC fragments from the Sardinia Channel used for U-series dating in this study (Table 1) as
212 well as sub-samples of the twenty-five CWC fragments originating from the Alboran Sea, which were already
213 radiocarbon-dated by Fink et al. (2013) (Table 2), were used for further Nd isotopic composition analyses. The
214 fragments (350 to 600 mg) were subjected to a mechanical and chemical cleaning procedure. The visible
215 contaminations, such as Fe-Mn coatings and detrital particles, were carefully removed from the inner and
216 outermost surfaces of the coral skeletons using a small diamond blade. The physically cleaned fragments were
217 ultrasonicated for 10 min with 0.1 N ultra-clean HCl, followed by several MilliQ water rinses and finally
218 dissolved in 2.5 N ultraclean HNO_3. Nd was separated from the carbonate matrix using Eichrom TRU and LN
219 resins, following the analytical procedure described in detail in Copard et al. (2010).
220 The ^{143}Nd/^{144}Nd ratios of all purified Nd fractions were analyzed using the ThermoScientific Neptune^{Plus} Multi-
221 Collector Inductively Coupled Plasma Mass Spectrometer (MC-ICP-MS) hosted at LSCE. The mass-
222 fractionation correction was made by normalizing ^{146}Nd/^{144}Nd to 0.7219 and applying an exponential law.
223 During each analytical session, samples were systematically bracketed with analyses of JNdi-1 and La Jolla
224 standard solutions, which are characterised by accepted values of 0.512115±0.000006 (Tanaka et al., 2000) and
225 0.511855±0.000007 (Lugmair et al., 1983), respectively. Standard JNdi-1 and La Jolla solutions were analysed
226 at concentrations similar to those of the samples (5-10 ppb) and all the measurements affected by instrumental
227 bias were corrected, when necessary, using La Jolla standard. The external reproducibility (2σ) for time resolved
228 measurement, deduced from repeated analyses of La Jolla and JNdi-1 standards, ranged from 0.1 to 0.5 εNd
229 units for the different analytical sessions. The analytical error for each sample analysis was taken as the external
230 reproducibility of the La Jolla standard for each session. Concentrations of Nd blanks were negligible compared
231 to the amount of Nd of CWC investigated in this study.

232

233 **3.3. Analyses on sediment of core SU92-33**
234   *3.3.1. Radiocarbon dating*
235 Radiocarbon dating was measured at UMS-ARTEMIS (Pelletron 3MV) AMS (CNRS-CEA Saclay, France).
236 Seven AMS radiocarbon (^{14}C) dating were performed in core SU92-33 on well-preserved calcareous tests of the
237 planktonic foraminifera *G. bulloides* in the size fraction >150 μm (Table 3). The age model for the core was
238 derived from the calibrated planktonic ages by applying a mean reservoir effect of ~400 years (Siani et al., 2000,
239 2001). All ^{14}C ages were converted to calendar years (cal. yr BP, BP = AD 1950) by using the INTCAL13
240 calibration data set (Reimer et al., 2013) and the CALIB 7.0 program (Stuiver and Reimer, 1993).

241

242   *3.3.2. Stable isotopes*
243 Stable oxygen (δ^{18}O) and carbon (δ^{13}C) isotope measurements were performed in core SU92-33 on well-
244 preserved (clean and intact) samples of the planktonic foraminifera *G. bulloides* (250-315 μm fraction) and the
245 epibenthic foraminifera *C. pachyderma* (250-315 μm fraction) using a Finnigan MAT-253 mass spectrometer at
246 the State Key Laboratory of Marine Geology (Tongji University). Both δ^{18}O and δ^{13}C values are presented

247 relative to the Pee Dee Belemnite (PDB) scale by comparison with the National Bureau of Standards (NBS) 18

248 and 19. The mean external reproducibility was checked by replicate analyses of laboratory standards and is better

249 than ±0.07‰ (1σ) for $\delta^{18}O$ and ±0.04‰ for $\delta^{13}C$.

250 *3.3.3 Nd isotope measurements on planktonic foraminifera*

251 Approximately 25 mg of mixed planktonic foraminifera species were picked from the >63 μm size fraction of

252 each sample already used for stable isotope measurements (Table 4). The samples were gently crushed between

253 glass slides under the microscope to ensure that all chambers were open, and ultrasonicated with MilliQ water.

254 Samples were allowed to settle between ultrasonication steps before removing the supernatant. Each sample was

255 rinsed thoroughly with MilliQ water until the solution was clear and free of clay. The cleaned samples were

256 dissolved in 1N acetic acid and finally centrifuged to ensure that all residual particles were removed, following

257 the procedure described in Roberts et al. (2010). Nd was separated following the analytical procedure reported in

258 Wu et al. (2015). For details on the measurement of Nd isotopes see the section above.

259

260 *3.3.4. Modern analogue technique (MAT)*

261 The palaeo-sea surface temperatures (SST) were estimated using the modern analogue technique (MAT)

262 (Hutson, 1980; Prell, 1985), implemented by Kallel et al. (1997) for the Mediterranean Sea. This method directly

263 measures the difference between the faunal composition of a fossil sample with a modern database, and it

264 identifies the best modern analogues for each fossil assemblage (Prell, 1985). Reliability of SST reconstructions

265 is estimated using a square chord distance test (dissimilarity coefficient), which represents the mean degree of

266 similarity between the sample and the best 10 modern analogues. When the dissimilarity coefficient is lower than

267 0.25, the reconstruction is considered to be of good quality (Overpeck et al., 1985; Kallel et al., 1997). For core

268 SU92-33, good dissimilarity coefficients are <0.2, with an average value of ~ 0.13 (varying between 0.07 and

269 0.19; Fig. 2a). The calculated mean standard deviation of SST estimates observed in core MD90-917 are ~ 1.5

270 °C from the late glacial period to the Younger Dryas and ~ 1.2 °C for the Holocene.

271

4. Results

4.1. Cold-water corals

274 The good state of preservation for the CWC samples from the Sardinia Channel (RECORD 23; Fig. 1) is attested

275 by their initial $\delta^{234}U$ values (Table 1), which is in the range of the modern seawater value (146.8±0.1; Andersen

276 et al., 2010). If the uncertainty of the $\delta^{234}U_i$ is taken into account, all the values fulfill the so-called "strict" ± 4

277 ‰ reliability criterion and the U/Th ages can be considered strictly reliable. The coral ages range from

278 0.091±0.011 to 10.904±0.042 ka BP (Table 1), and reveal three distinct clusters of coral age distribution during

279 the Holocene representing periods of sustained coral occurrence. These periods coincide with the Early Holocene

280 encompassing a 700-years-lasting time interval from ~10.9 to 10.2 ka BP, the very late Early Holocene at ~8.7

281 ka BP, and the Late Holocene starting at ~1.5 ka BP (Table 1).

282 Radiocarbon ages obtained for CWC samples collected in the Alboran Sea were published by Fink et al. (2013)

283 (Table 2). They also document three periods of sustained CWC occurrence coinciding with the Bølling–Allerød

284 (B-A) interstadial (13.5–12.9 cal ka BP), the Early Holocene (11.2–9.8 cal ka BP) and the Mid- to Late Holocene

285 (5.4–0.3 cal ka BP).

286   The εNd record obtained from the CWC samples from the Alboran Sea displays a narrow range from -9.22±0.30

287   to -8.59±0.3, which is comparable to the εNd record of the planktonic foraminifera from the Balearic Sea over

288   the last 13.5 kyr (Table 2, Fig. 3b). Most of the CWC εNd values are similar within error and the record does not

289   reveal any clear difference over the last ~13.5 kyr.

290   On the contrary, the CWC samples from the Sardinia Channel display a relatively large εNd range, with values

291   varying from -5.99±0.50 to -7.75±0.10 during the Early and Late Holocene, and values as low as -8.66±0.30

292   during the the mid-sapropel S1 deposition (S1a) at ~8.7 ka BP (Table 1, Fig. 3c).

293

294

295   ### 4.2 Core SU92-33

296   The stratigraphy of core SU92-33 was derived from the $\delta^{18}O$ variations of the planktonic foraminifera

297   *G. bulloides* (Fig. 2b). The last glacial/interglacial transition and the Holocene encompasses the upper 2.1 m of

298   the core (Fig. 2b). The $\delta^{18}O$ record of *G. bulloides* shows higher values (~3.5 ‰) during the late glacial

299   compared to the Holocene (from ~1.5 to 0.8 ‰) exhibiting a pattern similar to those observed in nearby deep-sea

300   cores from the Western Mediterranean Sea (Sierro et al., 2005; Melki et al., 2009).

301   The age model for the upper 1.2 m of the core SU92-33 was based on 7 AMS-^{14}C age measurements and a

302   linear interpolation between these ages (Table 3, Fig. 2). For the lower portion of the core, a control point was

303   established at the onset of the last deglaciation, which is coeval in the western and central Mediterranean Sea at

304   ~17 cal ka BP (Sierro et al., 2005; Melki et al., 2009; Siani et al., 2001). Overall, the upper 2.1 m of core SU92-

305   33 spans the last 19 kyr, with an estimated average sedimentation rate ranging from ~15 cm ka^{-1} during the

306   deglaciation to ~10 cm ka^{-1} during the Holocene.

307   April-May SST reconstruction was derived from MAT to define the main climatic events recorded in

308   core SU92-33 during the last 19 kyr. SST vary from 8.5°C to 17.5°C with high amplitude variability over the last

309   19 kyr BP (Fig. 2a). The LGM (19-18 ka BP) is characterized by SST values centered at around 12°C. Then, a

310   progressive decrease of ~4°C between 17.8 ka and 16 ka marks the Henrich Stadial 1 (HS1) (Fig. 2a). A

311   warming phase (~14°C) between 14.5 ka BP and 13.8 ka BP coincides with the B-A interstadial and is followed

312   by a cooling (~11°C) between 13.1 ka BP and 11.8 ka BP largely corresponding to the YD (Fig. 2a). During the

313   Holocene, SST show mainly values of ~16°C, with one exception between 7 ka BP and 6 ka BP pointing to an

314   abrupt cooling of ~3°C (Fig. 2a). From the late glacial to the Holocene, SST variations show a similar pattern to

315   that previously observed in the Gulf of Lions and Tyrrhenian Sea (Kallel et al., 1997; Melki et al., 2009) as well

316   as in the Alboran Sea (Martrat et al., 2014; Rodrigo-Gámiz et al., 2014). They are globally synchronous for the

317   main climatic transitions to the well dated South Adriatic Sea core MD90-917 (Siani et al., 2004) confirming the

318   robustness of the SU92-33 age model (Fig. 2a).

319   The $\delta^{18}O$ and $\delta^{13}C$ records obtained from the benthic foraminifera *C. pachyderma* display significant variations

320   at millennial time scales (Figs. 2c and 2d). The $\delta^{18}O$ values decrease steadily from ~4.5 ‰ during the LGM to

321   ~1.5 ‰ during the Holocene, without showing any significant excursion during HS1 and the YD events (Fig.

322   2c), in agreement with results obtained from the neighbor core MD99-2343 (Sierro et al., 2005).

323   The $\delta^{13}C$ record of *C. pachyderma* shows a decreasing trend since the LGM with a low variability from ~1.6 ‰

324   to ~0.6 ‰ (Fig. 2d). The heaviest $\delta^{13}C$ values are related to the LGM (~1.6 ‰) while the lightest values (~0.6

‰) characterize the Early Holocene and in particular the period corresponding to the sapropel S1 event in the eastern Mediterranean basin (Fig. 2d).

The εNd values of planktonic foraminifera of core SU92-33 from the Balearic Sea vary within a relatively narrow range between -9.50±0.30 and -8.61±0.30, with an average value of -9.06±0.28 (Table 2, Fig. 3b). The record shows a slight increasing trend since the LGM, with the more unradiogenic values (average -9.28±0.15; n=7) being observed in the oldest part of the record (between 18 and 13.5 ka BP), whereas Holocene values are generally more radiogenic (average -8.84±0.22; n=17) (Fig. 3b).

5. Discussion

Overall, the CWC and foraminiferal εNd values measured in this study point to a pronounced dispersion at intermediate depth in terms of absolute values and variability in Nd isotopes during the Holocene between the Alboran and Balearic Seas and the Sardinia Channel. Furthermore, the foraminiferal εNd record reveals an evolution towards more radiogenic values at intermediate water depth in the Balearic Sea over the last ~19 kyr (Fig. 3).

A prerequisite to properly interpret such εNd differences and variations through time consists in characterizing first the present-day εNd of the main water-mass end-members flowing in the western Mediterranean basin. It is also necessary to evaluate the temporal changes in εNd of the end-members since the LGM, and assess the potential influences of lithogenic Nd input and regional exchange between the continental margins and seawater ("boundary exchange"; Lacan and Jeandel, 2001, 2005) on the εNd values of intermediate water masses.

During its westward flow, the LIW continuously mixes with surrounding waters with different εNd signatures lying above and below. For the western Mediterranean basin, these water masses are the MAW/Western Intermediate Water (WIW) and the TDW/WMDW, respectively. Accordingly, a well-defined and gradual εNd gradient exists at intermediate depth between the eastern and western Mediterranean basins, with LIW values becoming progressively more unradiogenic towards the Strait of Gibraltar, from -4.8±0.2 at 227 m in the Levantine basin to -10.4±0.2 at 200 m in the Alboran Sea (Tachikawa et al., 2004). Such an εNd pattern implies an effective vertical mixing with more unradiogenetic water masses along the E-W LIW trajectory ruling out severe isotopic modifications of the LIW due to the local exchange between the continental margins and seawater. Unfortunately, no information exists on the potential temporal variability in εNd of the Mediterranean water-mass end-members since the LGM.

It has been demonstrated that eolian dust input can modify the surface and sub-surface εNd distribution of the ocean in some areas (Arsouze et al., 2009). The last glacial period was associated with an aridification of North Africa (Sarnthein et al., 1981; Hooghiemstra et al., 1987; Moreno et al., 2002; Wienberg et al., 2010) and higher fluxes of Saharan dust to the NE tropical Atlantic (Itambi et al., 2009) and the western Mediterranean Sea characterized by unradiogenic εNd values (between -11±0.4 and -14±0.4;; see synthesis in Scheuvens et al., 2013). Bout-Roumazeilles et al. (2013) documented a dominant role of eolian supply in the Siculo-Tunisian Strait during the last 20 ka, with the exception of a significant riverine contribution (from the Nile River) and a strong reduction of eolian input during the sapropel S1 event. Such variations in the eolian input to the Mediterranean Sea are not associated to a significant change in the seawater εNd record obtained for the Balearic Sea (core SU92-33) during the sapropel S1 event (Fig. 3). Furthermore, the εNd signature of the CWC from the Sardinia Channel (core RECORD 23) shifts to more unradiogenic values (-8.66±0.30) during the sapropel S1

365   event, which is opposite to what expected if it was related to a strong reduction of eolian sediment input. In a

366   recent study, Rodrigo-Gámiz et al. (2015) have documented variations in the terrigenous provenance from a

367   sediment record in the Alboran Sea (core 293G; 36°10.414'N, 2°45.280'W, 1840 m water depth) since the

368   LGM. Radiogenic isotopes (Sr, Nd, Pb) point to changes from North African dominated sources during the

369   glacial period to European dominated source during the Holocene. Nevertheless, the major Sr-Nd-Pb excursions

370   documented by Rodrigo-Gámiz et al. (2015) and dated at ca. 11.5, 10.2, 8.9-8.7, 5.6, 2.2 and 1.1. ka cal BP do

371   not seem to affect the εNd values of our foraminifera and coral records.

372   Taken together, these results suggest that changes of eolian dust input since the LGM were not responsible for

373   the observed εNd variability at intermediate water depths.

374   Consequently, assuming that the Nd isotopic budget of the western Mediterranean Sea has not been strongly

375   modified since the LGM, the reconstructed variations of the E-W gradient of εNd values in the western

376   Mediterranean Sea for the past and notably during the sapropel S1 event (Fig. 3) are indicative of a major

377   reorganization of intermediate water circulation.

378

379   *5.1 Hydrological changes in the Alboran and Balearic Seas since the LGM*

380   The range in εNd for the CWC from the Alboran Sea (from -9.22±0.30 to -8.8.59±0.30; Table 2) is very close to

381   the one obtained for the planktonic foraminifera from the Balearic Sea (from -9.50±0.30 to -8.61±0.30; Table 4,

382   Fig. 3c), suggesting that both sites are influenced by the same intermediate water masses at least for the last 13.5

383   kyr BP. Today, LIW occupies a depth range between ~200 and ~700 m in the western Mediterranean basin

384   (Millot, 1999; Sparnocchia et al., 1999). More specifically, the salinity maximum corresponding to the core of

385   LIW is found at around 400 m in the Alboran Sea (Millot, 2009) and up to 550 m in the Balearic Sea (López-

386   Jurado et al., 2008). The youngest CWC sample collected in the Alboran Sea with a rather "recent" age of 0.34

387   cal ka BP (Fink et al. 2013) displays an εNd value of -8.59±0.30 (Table 2) that is similar to the present-day value

388   of the LIW at the same site (-8.3±0.2) (Dubois-Dauphin et al., submitted) and is significantly different from the

389   WMDW εNd signature in the Alboran Sea (-10.7±0.2, 1270 m water depth; Tachikawa et al., 2004). Considering

390   the intermediate depth range of the studied CWC and foraminifera samples, we can reasonably assume that

391   samples from both sites, in the Balearic Sea (622 m water depth) and in the Alboran Sea (280 to 442 m water

392   depth), record εNd variations of the LIW. The εNd record obtained from planktonic foraminifera generally

393   displays more unradiogenic and homogenous values before ~13 cal ka BP (range from -9.46 to -9.12) compared

394   to the most recent part of the record (range from -9.50 to -8.61), with the highest value of -8.61±0.3 in the Early

395   and Late Holocene.

396   The SST record displays values centered at around 12°C during the LGM with a subsequent rapid SST decrease

397   towards 9°C , highlighting the onset of the HS1 (Fig. 2a). These values are well comparable to recent high-

398   resolution SST data obtained in the Alboran Sea (Martrat et al., 2014; Rodrigo-Gámiz et al., 2014).

399   The δ^{18}O record obtained on *G. bulloides* indicates an abrupt 1‰ excursion towards lighter values centered at

400   about 16 cal ka BP (Table 4), synchronous with the HS1 (Fig. 2b), which is similar to the δ^{18}O shift reported by

401   Sierro et al. (2005) for a core collected at 2391 m water depth NE of the Balearic Islands (MD99-2343; Fig. 1).

402   As the Heinrich events over the last glacial period are characterized by colder and fresher surface water in the

403   Alboran Sea (Cacho et al., 1999; Pérez-Folgado et al., 2003; Martrat et al., 2004, 2014; Rodrigo-Gámiz et al.,

404   2014) and dry climate on land over the western Mediterranean Sea (Allen et al., 1999; Combourieu-Nebout et

al., 2002; Sanchez Goni et al., 2002; Bartov et al., 2003), lighter $\delta^{18}O$ values of planktonic *G. bulloides* are thought to be the result of the inflow of freshwater derived from the melting of icebergs in the Atlantic Ocean into the Mediterranean Sea (Sierro et al., 2005; Rogerson et al., 2008).

During this time interval, the $\delta^{13}C$ record of *C. pachyderma* from the Balearic Sea (core SU92-33) displays a decreasing $\delta^{13}C$ trend after ~16 cal ka BP (from 1.4 ‰ to 0.9 ‰; Table 4; Fig. 4a). Moreover, the $\delta^{13}C$ record obtained on benthic foraminifera *C. pachyderma* from the deep Balearic Sea (core MD99-2343) reveals similar $\delta^{13}C$ values before ~16 cal ka BP suggesting well-mixed and ventilated water masses during the LGM and the onset of the deglaciation (Sierro et al., 2005).

The slightly lower foraminiferal εNd values before ~13 cal ka BP could reflect a stronger influence of water masses deriving from the Gulf of Lions as WMDW (εNd: -9.4±0.9; Henry et al., 1994; Tachikawa et al., 2004; Montagna, pers. comm., 2016). This is in agreement with εNd results obtained by Jiménez-Espejo et al. (2015) from planktonic foraminifera collected from deep-water sites (1989 m and 2382 m) in the Alboran Sea (Fig. 4c). Jiménez-Espejo et al. (2015) documented lower εNd values (ranging from -10.14±0.27 to -9.58±0.22) during the LGM, suggesting an intense deep-water formation. This is also associated to an enhanced activity of the deeper branch of the MOW in the Gulf of Cádiz (Rogerson et al., 2005; Voelker et al., 2006) linked to the active production of the WMDW in the Gulf of Lions during the LGM (Jiménez-Espejo et al., 2015).

The end of the HS1 (14.7 cal ka BP) is concurrent with the onset of the B-A warm interval characterized by increased SST up to 14°C in the Balearic Sea (SU92-33: Fig. 3a), also identified for various sites in the Mediterranean Sea (Cacho et al., 1999; Martrat et al., 2004, 2014; Essallami et al., 2007; Rodrigo-Gámiz et al., 2014). The B-A interval is associated with the so-called melt-water pulse 1A (e.g. Weaver et al., 2003) occurring at around 14.5 cal ka BP. This led to a rapid sea-level rise of about 20 m in less than 500 years and large freshwater discharges in the Atlantic Ocean due to the melting of continental ice sheets (Deschamps et al., 2012), resulting in an enhanced Atlantic inflow across the Strait of Gibraltar. Synchronously, cosmogenic dating of Alpine glacier retreat throughout the western Mediterranean hinterland suggests maximum retreat rates (Ivy-Ochs et al., 2007; Kelly et al., 2006). Overall, these events are responsible for freshening Mediterranean waters and reduced surface water density, and hence, weakened ventilation of intermediate (Toucanne et al., 2012) and deep-water masses (Cacho et al., 2000; Sierro et al., 2005). Similarly, lower benthic $\delta^{13}C$ values obtained for the Balearic Sea (Fig. 4a) point to less ventilated intermediate water relative to the late glacial. In addition, a decoupling in the benthic $\delta^{13}C$ values is observed between deep (MD99-2343) and intermediate (core SU92-33) waters after ~16 cal ka BP (Sierro et al. 2005), suggesting an enhanced stratification of the waters masses (Fig. 4a). At this time, the shallowest εNd record from the deep Alboran Sea (core 300G) shifted towards more radiogenic values, while the deepest one (core 304G) remained close to the LGM values (Jimenez-Espejo et al., 2015) (Fig. 4c). Furthermore, results from the UP10 fraction (particles > 10 μm) of the MD99-2343 sediment core (Fig. 4d) indicate a declining bottom-current velocity at 15 ka BP (Frigola et al., 2008). Rogerson et al. (2008) have hypothesized that during deglacial periods the sinking depth of dense waters produced in the Gulf of Lions was shallower resulting in new intermediate water (WIW) rather than new deep-water (WMDW) as observed today during mild winters (Millot, 1999; Schott et al., 1996). Therefore, intermediate depths of the Balearic Sea could have been isolated from the deep-water with the onset of the T1 (at ~15 ka BP). The reduced convection in the deep western Mediterranean Sea together with the shoaling of the nutricline (Rogerson et al., 2008) led to the deposition of the ORL 1 (14.5 to 8.2 ka B.P; Cacho et al., 2002) and dysoxic conditions below

445 2000 m in agreement with the absence of epibenthic foraminifera such as *C. pachyderma* after 11 cal ka BP in

446 MD99-2343 (Sierro et al., 2005) (Fig. 4a).

447 After 13.5 ka BP, planktonic foraminifera εNd values from the Balearic Sea (core SU92-33) become more

448 radiogenic and are in the range of CWC εNd values from the Alboran Sea (Fig. 4b). These values may reveal a

449 stronger influence of the LIW in the Balearic Sea during the Younger Dryas, as also supported by the sortable

450 silt record from the Tyrrhenian Sea (Toucanne et al., 2012) (Fig. 4e). Deeper depths of the Alboran Sea also

451 record a stronger influence of the LIW with an εNd value of -9.1±0.4 (Jimenez-Espejo et al., 2015). In addition,

452 a concomitant activation of the upper MOW branch, as reconstructed from higher values of Zr/Al ratio in

453 sediments of the Gulf of Cádiz, can be related to the enhanced LIW flow in the western Mediterranean Sea (Fig.

454 4f) (Bahr et al., 2015).

455 The time of sapropel S1 deposition (10.2 – 6.4 ka) is characterized by a weakening or a shutdown of

456 intermediate- and deep-water formation in the eastern Mediterranean basin (Rossignol-Strick et al., 1982; Cramp

457 and O'Sullivan, 1999; Emeis et al., 2000; Rohling et al., 2015). At this time, planktonic foraminifera εNd values

458 from intermediate water depths in the Balearic Sea (core SU92-33) remain high (between -9.15±0.3 and -

459 8.61±0.3) (Fig. 4b). On the other hand, the deeper Alboran Sea provides a value of -9.8±0.3 pointing to a

460 stronger contribution of WMDW (Jimenez-Espejo et al., 2015), coeval with the recovery of deep-water activity

461 from core MD99-2343 (Frigola et al., 2008).

462

463 *5.2 Hydrological changes in the Sardinia Channel during the Holocene*

464 The present-day hydrographic structure of the Sardinia Channel is characterized by four water masses, with the

465 surface, intermediate and deep-water masses being represented by MAW, LIW and TDW/WMDW, respectively

466 (Astraldi et al., 2002a; Millot and Taupier-Lepage, 2005). In addition, the WIW, flowing between the MAW and

467 the LIW, has also been observed along the Channel (Sammari et al., 1999). The core of the LIW is located at

468 400-450 m water depth in the Tyrrhenian Sea (Hopkins, 1988; Astraldi et al., 2002b), which is the depth range of

469 CWC samples from the Sardinia Channel (RECORD 23; 414 m) (Taviani et al., 2015). The youngest CWC

470 sample dated at ~0.1 ka BP has an εNd value of -7.70±0.10 (Table 1, Fig. 5), which is similar within error to the

471 value obtained from a seawater sample collected at 451 m close to the coral sampling location (-8.0±0.4;

472 Montagna, pers. comm., 2016).

473 The CWC dating from the Sardinia Channel shows three distinct periods of sustained coral occurrence in this

474 area during the Holocene, with each displaying a large variability in εNd values. CWC from the Early Holocene

475 (10.9-10.2 ka BP) and the Late Holocene (<1.5 ka BP) exhibit similar ranges of εNd values (ranging from -

476 5.99±0.50 to -7.75±0.20; Table 1, Fig 5c). Such variations are within the present-day εNd range being

477 characteristic for intermediate waters in the eastern Mediterranean Sea (-6.6±1.0; Tachikawa et al., 2004; Vance

478 et al., 2004). However, the CWC εNd values are more radiogenic than those observed at mid-depth in the

479 present-day western basin (ranging from -10.4±0.2 to -7.58 ±0.47; Henry et al., 1994; Tachikawa et al., 2004;

480 Montagna, pers. comm., 2016), suggesting a stronger LIW component in the Sardinia Channel during the Early

481 and Late Holocene. The Sardinian CWC εNd variability also reflects the sensitivity of the LIW to changes in the

482 eastern basin such as rapid variability of the Nile River flood discharge (Revel et al., 2014; 2015; Weldeab et al.,

483 2014) or a modification through time in the proportion between the LIW and the Cretan Intermediate Water

484 (CIW). Today, the intermediate water outflowing from the Strait of Sicily is composed by ~66 to 75 % of LIW

485 and 33 to 25 % of CIW (Manca et al., 2006; Millot, 2014). As the CIW is formed in the Aegean Sea, this
486 intermediate water mass is generally more radiogenic than LIW (Tachikawa et al., 2004; Montagna, pers.
487 comm., 2016). Following this hypothesis, a modification of the mixing proportion between the CIW and the
488 LIW may potentially explain values as radiogenic as about -6 in the Sardinia Channel during the Early and Late
489 Holocene (Fig. 5c). However, a stronger LIW and/or a CIW contribution cannot be responsible for εNd values as
490 low as -8.66±0.30 observed during the sapropel S1 event at 8.7 ka BP (Table 1, Fig. 5c). Considering that such
491 unradiogenic value is not observed at intermediate depth in the modern eastern Mediterranean basin, the most
492 plausible hypothesis suggested here is that the CWC were influenced by a higher contribution of intermediate
493 water from the western basin.
494
495 ### 5.3 Hydrological implications for the intermediate water masses of the western Mediterranean Sea
496 The εNd records of the Balearic Sea, Alboran Sea and Sardinia Channel document a temporal variability of the
497 east-west gradient in the western Mediterranean basin during the Holocene. The magnitude of the gradient
498 ranges from ~1.5 to ~3 ε units during the Early and Late Holocene and it is strongly reduced at 8.7 ka BP,
499 coinciding with the sapropel S1 event affecting the eastern Mediterranean basin (Fig. 5). Such variations could
500 be the result of a modification of the Nd isotopic composition of intermediate water masses due to changes of the
501 LIW production through time and a higher contribution of the western-sourced intermediate water towards the
502 Sardinia Channel coinciding with the sapropel S1 event.
503 The LIW acquires its radiogenic εNd in the Mediterranean Levantine basin mainly from Nd exchange between
504 seawater and lithogenic particles originating mainly from Nile River (Tachikawa et al., 2004). A higher sediment
505 supply from the Nile River starting at ~15 ka BP was documented by a shift to more radiogenic εNd values of
506 the terrigenous fraction obtained from a sediment core having been influenced by the Nile River discharge
507 (Revel et al., 2015) (Fig. 5e). Others studies pointed to a gradual enhanced Nile River runoff as soon as 14.8 ka
508 BP and a peak of Nile discharge from 9.7 to 8.4 ka recorded by large increase in sedimentation rate from 9.7 to
509 8.4 ka (>120 cm/ka) (Revel et al., 2015; Weldeab et al., 2014; Castaneda et al., 2016). Similarly, enhanced Nile
510 discharge at ~9.5 cal kyr B.P was inferred based on $\delta^{18}O$ in planktonic foraminifera from a sediment core in the
511 southeast Levantine Basin (PS009PC (32°07.7′N, 34°24.4′E; 552 m water depth) (Hennekam et al., 2014). This
512 increasing contribution of the Nile River to the eastern Mediterranean basin has been related to the African
513 Humid Period (14.8–5.5 ka BP; Shanahan et al., 2015), which in turn was linked to the precessional increase in
514 Northern Hemisphere insolation during low eccentricity (deMenocal et al., 2000; Barker et al., 2004; Garcin et
515 al., 2009). An increasing amount of radiogenic sediments dominated by the Blue/Atbara Nile River contribution
516 (Revel et al., 2014) could have modified the εNd of surface water towards more radiogenic values (Revel, pers.
517 comm., 2016). Indeed, planktonic foraminifera εNd values as high as ~ -3 have been documented in the eastern
518 Levantine Basin (ODP site 967; 34°04.27′N, 32°43.53′E; 2553 m water depth) during the sapropel S1 event as a
519 result of enhanced Nile flooding (Scrivner et al., 2004). The radiogenic signature was likely transferred to
520 intermediate depth as a consequence of the LIW formation in the Rhodes Gyre, and it might have been
521 propagated westwards towards the Sardinia Channel.
522 Therefore, considering the more unradiogenic value of the CWC samples from the Sardinia Channel during the
523 sapropel S1a event, it is very unlikely that eastern-sourced water flowed at intermediate depth towards the
524 Sardinia Channel. A possible explanation could be the replacement of the radiogenic LIW that was no longer

525   produced in the eastern basin (Rohling, 1994) by less radiogenic western intermediate water (possibly WIW).
526   Such a scenario could even support previous hypotheses that invoke a potential circulation reversal in the eastern
527   Mediterranean from anti-estuarine to estuarine during sapropel formation (Huang and Stanley, 1972; Calvert,
528   1983; Sarmiento et al., 1988; Buckley and Johnson, 1988; Thunell and Williams, 1989). An alternative
529   hypothesis would be that reduced surface water densities in the eastern Mediterranean during sapropel S1
530   resulted in the LIW sinking to shallower depths than at present. As a result of this shoaling, CWC from the
531   Sardinia Channel would have been bathed by underlying Western Intermediate Water during the sapropel S1a
532   event.

6. Conclusions

535   The foraminiferal εNd record from intermediate depths in the Balearic Sea reveals a relatively narrow range of
536   εNd values varying between -9.50 and -8.61 since the LGM (~20 ka). Between 18 and 13.5 cal ka BP, the more
537   unradiogenic εNd values support a vigorous deep overturning in the Gulf of Lions while δ^{18}O and δ^{13}C values
538   indicate a stratification of the water masses after 16 cal ka BP. The stratification together with a decrease of the
539   deep-water intensity led to more radiogenic values after ~13 cal ka BP. The foraminiferal εNd record, supported
540   by εNd values from CWC in the Alboran Sea, shows only minor changes in neodymium isotopes from 13.5 cal
541   ka BP to 0.34 cal ka BP, suggesting that the westernmost part of the western Mediterranean basin is not very
542   sensitive to hydrological variations of the LIW.

543   On the contrary, CWC located at the depth of the LIW in the Sardinia Channel exhibit large εNd variations
544   (between -7.75±0.10 and -5.99±0.50) during the Holocene, suggesting either the role of the Nile River in
545   changing the εNd of the LIW in the eastern Mediterranean basin or a variable LIW/CIW mixing of the water
546   outflowing from the Strait of Sicily. At the time of the sapropel S1 event at ~8.7 ka BP, CWC display a shift
547   toward lower values (-8.66±0.30), similar to those obtained at intermediate depths in the westernmost part of the
548   western basin. This suggests that western-sourced intermediate water likely filled mid-depth of the southern
549   Sardinia, replacing LIW that was no longer produced (or heavily reduced) in the eastern basin. These results
550   could potentially support a reversal of the Mediterranean circulation, although this assumption needs further
551   investigation to be confirmed.

Acknowledgements
The research leading to this study has received funding from the French National Research Agency
"Investissement d'Avenir" (n°ANR-10-LABX-0018), the HAMOC project ANR-13-BS06-0003, the
MISTRALS/PALEOMEX/COFIMED and ENVIMED/Boron Isotope and Trace Elements project. This work
contributes to the RITMARE project. We thank Hiske Fink for selecting and kindly providing the cold-water
corals samples from the Alboran Sea. We further thank François Thil and Louise Bordier for their support with
Nd isotopic composition analyses. Paolo Montagna is grateful for financial support from the Short Term
Mobility Program (CNR). Thanks are also extended to the captains, crews, chief scientists, and scientific parties
of research cruises RECORD (R/V Urania), POS-385 (R/V Poseidon) and PALEOCINAT II (R/V Le Suroît).

References

Abu-Zied, R. H., Rohling, E. J., Jorissen, F. J., Fontanier, C., Casford, J. S. L. and Cooke, S.: Benthic foraminiferal response to changes in bottom-water oxygenation and organic carbon flux in the eastern Mediterranean during LGM to Recent times, Mar. Micropaleontol., 67(1-2), 46–68, doi:10.1016/j.marmicro.2007.08.006, 2008.

Allen, J. R. M., Huntley, B., Brandt, U., Brauer, A., Hubberten, H., Keller, J., Kraml, M., Mackensen, A., Mingram, J., Negendank, J. F. W., Nowaczyk, N. R., Oberhänsli, H., Watts, W. A., Wulf, S. and Zolitschka, B.: Rapid environmental changes in southern Europe during the last glacial period, Nature, 400(6746), 740–743, doi:10.1038/23432, 1999.

Andersen, M. B., Stirling, C. H., Zimmermann, B. and Halliday, A. N.: Precise determination of the open ocean 234U/238U composition, Geochemistry, Geophys. Geosystems, 11(12), Q12003, doi:10.1029/2010GC003318, 2010.

Arsouze, T., Dutay, J.-C., Lacan, F. and Jeandel, C.: Reconstructing the Nd oceanic cycle using a coupled dynamical – biogeochemical model, Biogeosciences, 6(12), 2829–2846, doi:10.5194/bg-6-2829-2009, 2009.

Astraldi, M., Gasparini, G. P., Gervasio, L. and Salusti, E.: Dense Water Dynamics along the Strait of Sicily (Mediterranean Sea), J. Phys. Oceanogr., 31(12), 3457–3475, doi:10.1175/1520-0485(2001)031<3457:DWDATS>2.0.CO;2, 2001.

Astraldi, M., Gasparini, G. P., Vetrano, A. and Vignudelli, S.: Hydrographic characteristics and interannual variability of water masses in the central Mediterranean: A sensitivity test for long-term changes in the Mediterranean Sea, Deep. Res. Part I Oceanogr. Res. Pap., 49(4), 661–680, doi:10.1016/S0967-0637(01)00059-0, 2002a.

Astraldi, M., Conversano, F., Civitarese, G., Gasparini, G. P., Ribera d'Alcalà, M. and Vetrano, a.: Water mass properties and chemical signatures in the central Mediterranean region, J. Mar. Syst., 33-34, 155–177, doi:10.1016/S0924-7963(02)00057-X, 2002b.

Bahr, A., Kaboth, S., Jiménez-Espejo, F. J., Sierro, F. J., Voelker, A. H. L., Lourens, L., Röhl, U., Reichart, G. J., Escutia, C., Hernández-Molina, F. J., Pross, J. and Friedrich, O.: Persistent monsoonal forcing of Mediterranean Outflow Water dynamics during the late Pleistocene, Geology, 43(11), 951–954, doi:10.1130/G37013.1, 2015.

Barker, P. A., Talbot, M. R., Street-Perrott, F. A., Marret, F., Scourse, J. and Odada, E. O.: Late Quaternary climatic variability in intertropical Africa, in Past Climate Variability through Europe and Africa, pp. 117–138, Springer Netherlands, Dordrecht., 2004.

Bartov, Y., Goldstein, S. L., Stein, M. and Enzel, Y.: Catastrophic arid episodes in the Eastern Mediterranean linked with the North Atlantic Heinrich events, Geology, 31(5), 439, doi:10.1130/0091-7613(2003)031<0439:CAEITE>2.0.CO;2, 2003.

597 Bigg, G. R. and Wadley, M. R.: Millennial-scale variability in the oceans: an ocean modelling view, J. Quat.
598 Sci., 16(4), 309–319, doi:10.1002/jqs.599, 2001.

599 Bout-Roumazeilles, V., Combourieu-Nebout, N., Desprat, S., Siani, G., Turon, J. L. and Essallami, L.: Tracking
600 atmospheric and riverine terrigenous supplies variability during the last glacial and the Holocene in central
601 Mediterranean, Clim. Past, 9(3), 1065–1087, doi:10.5194/cp-9-1065-2013, 2013.

602 Buckley, H. A. and Johnson, L. R.: Late pleistocene to recent sediment deposition in the central and western
603 Mediterranean, Deep Sea Res. Part A. Oceanogr. Res. Pap., 35(5), 749–766, doi:10.1016/0198-0149(88)90028-
604 3, 1988.

605 Cacho, I., Pelejero, C., Grimalt, J. O., Calafat, A. and Canals, M.: C37 alkenone measurements of sea surface
606 temperature in the Gulf of Lions (NW Mediterranean), Org. Geochem., 30(7), 557–566, doi:10.1016/S0146-
607 6380(99)00038-8, 1999.

608 Cacho, I., Grimalt, J. O., Sierro, F. J., Shackleton, N. and Canals, M.: Evidence for enhanced Mediterranean
609 thermohaline circulation during rapid climatic coolings, Earth Planet. Sci. Lett., 183(3-4), 417–429,
610 doi:10.1016/S0012-821X(00)00296-X, 2000.

611 Cacho, I., Grimalt, J. O., Canals, M., Sbaffi, L., Shackleton, N. J., Schönfeld, J. and Zahn, R.: Variability of the
612 western Mediterranean Sea surface temperature during the last 25,000 years and its connection with the Northern
613 Hemisphere climatic changes, Paleoceanography, 16(1), 40–52, doi:10.1029/2000PA000502, 2001.

614 Cacho, I., Grimalt, J. O. and Canals, M.: Response of the Western Mediterranean Sea to rapid climatic variability
615 during the last 50,000 years: a molecular biomarker approach, J. Mar. Syst., 33-34, 253–272,
616 doi:10.1016/S0924-7963(02)00061-1, 2002.

617 Cacho, I., Shackleton, N., Elderfield, H., Sierro, F. J. and Grimalt, J. O.: Glacial rapid variability in deep-water
618 temperature and δ18O from the Western Mediterranean Sea, Quat. Sci. Rev., 25(23-24), 3294–3311,
619 doi:10.1016/j.quascirev.2006.10.004, 2006.

620 Calvert, S. E.: Geochemistry of Pleistocene sapropels and associated sediments from the Eastern Mediterranean,
621 Oceanol. Acta, 6(3), 255–267, 1983.

622 Castañeda, I. S., Schouten, S., Pätzold, J., Lucassen, F., Kasemann, S., Kuhlmann, H. and Schefuß, E.:
623 Hydroclimate variability in the Nile River Basin during the past 28,000 years, Earth Planet. Sci. Lett., 438, 47–
624 56, doi:10.1016/j.epsl.2015.12.014, 2016.

625 Cheng, H., Lawrence Edwards, R., Shen, C.-C., Polyak, V. J., Asmerom, Y., Woodhead, J. D., Hellstrom, J.,
626 Wang, Y., Kong, X., Spötl, C., Wang, X. and Calvin Alexander, E.: Improvements in 230Th dating, 230Th and
627 234U half-life values, and U–Th isotopic measurements by multi-collector inductively coupled plasma mass
628 spectrometry, Earth Planet. Sci. Lett., 371-372, 82–91, doi:10.1016/j.epsl.2013.04.006, 2013.

629 Colin, C., Frank, N., Copard, K. and Douville, E.: Neodymium isotopic composition of deep-sea corals from the
630 NE Atlantic: implications for past hydrological changes during the Holocene, Quat. Sci. Rev., 29(19-20), 2509–

631   2517, doi:10.1016/j.quascirev.2010.05.012, 2010.

632   Combourieu-Nebout, N., Turon, J. L., Zahn, R., Capotondi, L., Londeix, L. and Pahnke, K.: Enhanced aridity
633   and atmospheric high-pressure stability over the western Mediterranean during the North Atlantic cold events of
634   the past 50 k.y, Geology, 30(10), 863–866, doi:10.1130/0091-7613(2002)030<0863:EAAAHP>2.0.CO;2, 2002.

635   Copard, K., Colin, C., Douville, E., Freiwald, A., Gudmundsson, G., De Mol, B. and Frank, N.: Nd isotopes in
636   deep-sea corals in the North-eastern Atlantic, Quat. Sci. Rev., 29(19-20), 2499–2508,
637   doi:10.1016/j.quascirev.2010.05.025, 2010.

638   Copard, K., Colin, C., Henderson, G. M., Scholten, J., Douville, E., Sicre, M.-A. and Frank, N.: Late Holocene
639   intermediate water variability in the northeastern Atlantic as recorded by deep-sea corals, Earth Planet. Sci. Lett.,
640   313-314, 34–44, doi:10.1016/j.epsl.2011.09.047, 2012.

641   Cramp, A. and O'Sullivan, G.: Neogene sapropels in the Mediterranean: a review, Mar. Geol., 153(1-4), 11–28,
642   doi:10.1016/S0025-3227(98)00092-9, 1999.

643   De Lange, G. J., Thomson, J., Reitz, A., Slomp, C. P., Principato, M. S., Erba, E. and Corselli, C.: Synchronous
644   basin-wide formation and redox-controlled preservation of a Mediterranean sapropel, Nat. Geosci., 1(9), 606–
645   610, 2008.

646   DeMenocal, P., Ortiz, J., Guilderson, T. and Sarnthein, M.: Coherent High- and Low-Latitude Climate
647   Variability During the Holocene Warm Period, Science (80-.)., 288(5474), 2198–2202,
648   doi:10.1126/science.288.5474.2198, 2000.

649   Deschamps, P., Durand, N., Bard, E., Hamelin, B., Camoin, G., Thomas, A. L., Henderson, G. M., Okuno, J. and
650   Yokoyama, Y.: Ice-sheet collapse and sea-level rise at the Bølling warming 14,600 years ago, Nature,
651   483(7391), 559–564, doi:10.1038/nature10902, 2012.

652   Douville, E., Sallé, E., Frank, N., Eisele, M., Pons-Branchu, E. and Ayrault, S.: Rapid and accurate U–Th dating
653   of ancient carbonates using inductively coupled plasma-quadrupole mass spectrometry, Chem. Geol., 272(1-4),
654   1–11, doi:10.1016/j.chemgeo.2010.01.007, 2010.

655   Dubois-Dauphin, Q., Colin, C., Bonneau, L., Montagna, P., Wu, Q., Van Rooij, D., Reverdin, G., Douville, E.,
656   Thil, F., Waldner, A., Frank, N.: Fingerprinting North-east Atlantic water masses using Neodymium isotopes,
657   GCA, Submitted.
658

659   Elmore, A. C., Piotrowski, A. M., Wright, J. D. and Scrivner, A. E.: Testing the extraction of past seawater Nd
660   isotopic composition from North Atlantic deep sea sediments and foraminifera, Geochemistry, Geophys.
661   Geosystems, 12(9), doi:10.1029/2011GC003741, 2011.

662   Emeis, K.-C., Sakamoto, T., Wehausen, R. and Brumsack, H.-J.: The sapropel record of the eastern
663   Mediterranean Sea — results of Ocean Drilling Program Leg 160, Palaeogeogr. Palaeoclimatol. Palaeoecol.,
664   158(3-4), 371–395, doi:10.1016/S0031-0182(00)00059-6, 2000.

665 Fink, H. G., Wienberg, C., De Pol-Holz, R., Wintersteller, P. and Hebbeln, D.: Cold-water coral growth in the
666 Alboran Sea related to high productivity during the Late Pleistocene and Holocene, Mar. Geol., 339, 71–82,
667 doi:10.1016/j.margeo.2013.04.009, 2013.

668 Frigola, J., Moreno, A., Cacho, I., Canals, M., Sierro, F. J., Flores, J. a., Grimalt, J. O., Hodell, D. a. and Curtis,
669 J. H.: Holocene climate variability in the western Mediterranean region from a deepwater sediment record,
670 Paleoceanography, 22(2), n/a–n/a, doi:10.1029/2006PA001307, 2007.

671 Frigola, J., Moreno, A., Cacho, I., Canals, M., Sierro, F. J., Flores, J. A. and Grimalt, J. O.: Evidence of abrupt
672 changes in Western Mediterranean Deep Water circulation during the last 50kyr: A high-resolution marine
673 record from the Balearic Sea, Quat. Int., 181(1), 88–104, doi:10.1016/j.quaint.2007.06.016, 2008.

674 Garcin, Y., Junginger, A., Melnick, D., Olago, D. O., Strecker, M. R. and Trauth, M. H.: Late Pleistocene–
675 Holocene rise and collapse of Lake Suguta, northern Kenya Rift, Quat. Sci. Rev., 28(9-10), 911–925,
676 doi:10.1016/j.quascirev.2008.12.006, 2009.

677 Hebbeln, D, Wienberg, C, Beuck, L, Freiwald, A, Wintersteller, P and cruise participants (2009) Report and
678 preliminary results of R/V POSEIDON Cruise 385 "Cold-water corals of the Alboran Sea (western
679 Mediterranean Sea)", Faro - Toulon, 29.5. - 16.6.2009. Reports of the Department of Geosciences at the
680 University of Bremen, No. 273. Department of Geosciences, Bremen University. urn:nbn:de:gbv:46-
681 ep000106508.

682 Hennekam, R., Jilbert, T., Schnetger, B. and De Lange, G. J.: Solar forcing of Nile discharge and sapropel S1
683 formation in the early to middle Holocene eastern Mediterranean, Paleoceanography, 29(5), 343–356,
684 doi:10.1002/2013PA002553, 2014.

685 Henry, F., Jeandel, C., Dupré, B. and Minster, J.-F.: Particulate and dissolved Nd in the western Mediterranean
686 Sea: Sources, fate and budget, Mar. Chem., 45(4), 283–305, doi:10.1016/0304-4203(94)90075-2, 1994.

687 Hooghiemstra, H., Bechler, A. and Beug, H.-J.: Isopollen maps for 18,000 years B.P. of the Atlantic offshore of
688 northwest Africa: Evidence for paleowind circulation, Paleoceanography, 2, 561–582,
689 doi:10.1029/PA002i006p00561, 1987.

690 Hopkins, T. S.: Recent observations on the intermediate and deep water circulation in the Southern Tyrrhenian
691 Sea, Oceanol. Acta, (Special issue), 41–50, 1988.

692 Huang, T. C. and Stanley, D. J.: Western Alboran sea: sediment dispersal, pounding and reversal of currents, in
693 The Mediterranean Sea: A Natural Sedimentation Laboratory, pp. 521–559, Dowden, Hutchinson & Ross,
694 Stroudsurg, PA., 1972.

695 Hutson, W. H.: The Agulhas Current During the Late Pleistocene: Analysis of Modern Faunal Analogs, Science
696 (80-.)., 207(4426), 64–66, doi:10.1126/science.207.4426.64, 1980.

697 Itambi, a. C., von Dobeneck, T., Mulitza, S., Bickert, T. and Heslop, D.: Millennial-scale northwest African
698 droughts related to Heinrich events and Dansgaard-Oeschger cycles: Evidence in marine sediments from

699   offshore Senegal, Paleoceanography, 24(1), PA1205, doi:10.1029/2007PA001570, 2009.

700   Ivy-Ochs, S., Kerschner, H. and Schlüchter, C.: Cosmogenic nuclides and the dating of Lateglacial and Early
701   Holocene glacier variations: The Alpine perspective, Quat. Int., 164-165, 53–63,
702   doi:10.1016/j.quaint.2006.12.008, 2007.

703   Jacobsen, S. B. and Wasserburg, G. J.: Sm-Nd isotopic evolution of chondrites, Earth Planet. Sci. Lett., 50(1),
704   139–155, doi:10.1016/0012-821X(80)90125-9, 1980.

705   Jaffey, A. H., Flynn, K. F., Glendenin, L. E., Bentley, W. C. and Essling, A. M.: Precision measurements of half-
706   lives and specific activities of 235U and 238U, Phys. Rev. C, 4(5), 1889–1906, doi:10.1103/PhysRevC.4.1889,
707   1971.

708   Jiménez-Espejo, F. J., Pardos-Gené, M., Martínez-Ruiz, F., García-Alix, A., van de Flierdt, T., Toyofuku, T.,
709   Bahr, A. and Kreissig, K.: Geochemical evidence for intermediate water circulation in the westernmost
710   Mediterranean over the last 20kyrBP and its impact on the Mediterranean Outflow, Glob. Planet. Change, 135,
711   38–46, doi:10.1016/j.gloplacha.2015.10.001, 2015.

712   Kallel, N., Paterne, M., Labeyrie, L., Duplessy, J.-C. and Arnold, M.: Temperature and salinity records of the
713   Tyrrhenian Sea during the last 18,000 years, Palaeogeogr. Palaeoclimatol. Palaeoecol., 135(1-4), 97–108,
714   doi:10.1016/S0031-0182(97)00021-7, 1997.

715   Kelly, M. A., Ivy-Ochs, S., Kubik, P. W., Von Blanckenburg, F. and Schlüchter, C.: Chronology of deglaciation
716   based on 10 Be dates of glacial erosional features in the Grimsel Pass region, central Swiss Alps, Boreas, 35(4),
717   634–643, doi:10.1111/j.1502-3885.2006.tb01169.x, 2006.

718   Khelifi, N., Sarnthein, M., Andersen, N., Blanz, T., Frank, M., Garbe-Schonberg, D., Haley, B. a., Stumpf, R.
719   and Weinelt, M.: A major and long-term Pliocene intensification of the Mediterranean outflow, 3.5-3.3 Ma ago,
720   Geology, 37(9), 811–814, doi:10.1130/G30058A.1, 2009.

721   Kinder, T. H. and Parrilla, G.: Yes, some of the Mediterranean water does come from great depth, J. Geophys.
722   Res., 92, 2901–2906, doi:10.1029/JC092iC03p02901, 1987.

723   Kuhnt, T., Schmiedl, G., Ehrmann, W., Hamann, Y. and Hemleben, C.: Deep-sea ecosystem variability of the
724   Aegean Sea during the past 22 kyr as revealed by Benthic Foraminifera, Mar. Micropaleontol., 64(3-4), 141–
725   162, doi:10.1016/j.marmicro.2007.04.003, 2007.

726   Kuhnt, T., Schmiedl, G., Ehrmann, W., Hamann, Y. and Andersen, N.: Stable isotopic composition of Holocene
727   benthic foraminifers from the Eastern Mediterranean Sea: Past changes in productivity and deep water
728   oxygenation, Palaeogeogr. Palaeoclimatol. Palaeoecol., 268(1-2), 106–115, doi:10.1016/j.palaeo.2008.07.010,
729   2008.

730   Lacan, F. and Jeandel, C.: Tracing Papua New Guinea imprint on the central Equatorial Pacific Ocean using
731   neodymium isotopic compositions and Rare Earth Element patterns, Earth Planet. Sci. Lett., 186(3-4), 497–512,
732   doi:10.1016/S0012-821X(01)00263-1, 2001.

733 Lacan, F. and Jeandel, C.: Neodymium isotopes as a new tool for quantifying exchange fluxes at the continent–
734 ocean interface, Earth Planet. Sci. Lett., 232(3-4), 245–257, doi:10.1016/j.epsl.2005.01.004, 2005.

735 Lascaratos, A. and Nittis, K.: A high-resolution three-dimensional numerical study of intermediate water
736 formation in the Levantine Sea, J. Geophys. Res., 103(C9), 18497, doi:10.1029/98JC01196, 1998.

737 Lascaratos, A., Williams, R. G. and Tragou, E.: A mixed-layer study of the formation of Levantine intermediate
738 water, J. Geophys. Res., 98(C8), 14739, doi:10.1029/93JC00912, 1993.

739 López Correa, M., Montagna, P., Joseph, N., Rüggeberg, A., Fietzke, J., Flögel, S., Dorschel, B., Goldstein, S.
740 L., Wheeler, A. and Freiwald, A.: Preboreal onset of cold-water coral growth beyond the Arctic Circle revealed
741 by coupled radiocarbon and U-series dating and neodymium isotopes, Quat. Sci. Rev., 34, 24–43,
742 doi:10.1016/j.quascirev.2011.12.005, 2012.

743 López-Jurado, J. L., Marcos, M. and Monserrat, S.: Hydrographic conditions affecting two fishing grounds of
744 Mallorca island (Western Mediterranean): during the IDEA Project (2003-2004), J. Mar. Syst., 71(3-4), 303–
745 315, doi:10.1016/j.jmarsys.2007.03.007, 2008.

746 Ludwig, K. R. and Titterington, D. M.: Calculation of 230Th/U isochrons, ages, and errors, Geochim.
747 Cosmochim. Acta, 58(22), 5031–5042, doi:http://dx.doi.org/10.1016/0016-7037(94)90229-1, 1994.

748 Lugmair, G. W., Shimamura, T., Lewis, R. S. and Anders, E.: Samarium-146 in the Early Solar System:
749 Evidence from Neodymium in the Allende Meteorite, Science (80-.)., 222(4627), 1015–1018,
750 doi:10.1126/science.222.4627.1015, 1983.

751 Malanotte-Rizzoli, P., Manca, B. B., D'Alcala, M. R., Theocharis, A., Brenner, S., Budillon, G. and Ozsoy, E.:
752 The Eastern Mediterranean in the 80s and in the 90s: the big transition in the intermediate and deep circulations,
753 Dyn. Atmos. Ocean., 29(2-4), 365–395, doi:10.1016/S0377-0265(99)00011-1, 1999.

754 Manca, B., Ibello, V., Pacciaroni, M., Scarazzato, P. and Giorgetti, A.: Ventilation of deep waters in the Adriatic
755 and Ionian Seas following changes in thermohaline circulation of the Eastern Mediterranean, Clim. Res., 31,
756 239–256, doi:10.3354/cr031239, 2006.

757 Martrat, B., Grimalt, J. O., Lopez-Martinez, C., Cacho, I., Sierro, F. J., Flores, J. A., Zahn, R., Canals, M.,
758 Curtis, J. H. and Hodell, D. a: Abrupt temperature changes in the Western Mediterranean over the past 250,000
759 years., Science (80-.)., 306(5702), 1762–1765, doi:10.1126/science.1101706, 2004.

760 Martrat, B., Jimenez-Amat, P., Zahn, R. and Grimalt, J. O.: Similarities and dissimilarities between the last two
761 deglaciations and interglaciations in the North Atlantic region, Quat. Sci. Rev., 99, 122–134,
762 doi:10.1016/j.quascirev.2014.06.016, 2014.

763 Melki, T., Kallel, N., Jorissen, F. J., Guichard, F., Dennielou, B., Berné, S., Labeyrie, L. and Fontugne, M.:
764 Abrupt climate change, sea surface salinity and paleoproductivity in the western Mediterranean Sea (Gulf of
765 Lion) during the last 28 kyr, Palaeogeogr. Palaeoclimatol. Palaeoecol., 279(1-2), 96–113,
766 doi:10.1016/j.palaeo.2009.05.005, 2009.

767

768   Mercone, D., Thomson, J., Croudace, I. W., Siani, G., Paterne, M. and Troelstra, S.: Duration of S1, the most
769   recent sapropel in the eastern Mediterranean Sea, as indicated by accelerator mass spectrometry radiocarbon and
770   geochemical evidence, Paleoceanography, 15(3), 336–347, doi:10.1029/1999PA000397, 2000.

771   Mercone, D., Thomson, J., Abu-Zied, R. H., Croudace, I. W. and Rohling, E. J.: High-resolution geochemical
772   and micropalaeontological profiling of the most recent eastern Mediterranean sapropel, Mar. Geol., 177(1-2),
773   25–44, doi:10.1016/S0025-3227(01)00122-0, 2001.

774   Millot, C.: Circulation in the Western Mediterranean Sea, J. Mar. Syst., 20(1-4), 423–442, doi:10.1016/S0924-
775   7963(98)00078-5, 1999.

776   Millot, C.: Another description of the Mediterranean Sea outflow, Prog. Oceanogr., 82(2), 101–124,
777   doi:10.1016/j.pocean.2009.04.016, 2009.

778   Millot, C.: Heterogeneities of in- and out-flows in the Mediterranean Sea, Prog. Oceanogr., 120, 254–278,
779   doi:10.1016/j.pocean.2013.09.007, 2014.

780   Millot, C. and Taupier-Letage, I.: Circulation in the Mediterranean Sea, in Environmental Chemistry, vol. 5,
781   edited by A. Saliot, pp. 29–66, Springer Berlin Heidelberg, Heidelberg., 2005.

782   Millot, C., Candela, J., Fuda, J.-L. and Tber, Y.: Large warming and salinification of the Mediterranean outflow
783   due to changes in its composition, Deep Sea Res. Part I Oceanogr. Res. Pap., 53(4), 656–666,
784   doi:10.1016/j.dsr.2005.12.017, 2006.

785   Montero-Serrano, J.-C., Frank, N., Colin, C., Wienberg, C. and Eisele, M.: The climate influence on the mid-
786   depth Northeast Atlantic gyres viewed by cold-water corals, Geophys. Res. Lett., 38(19),
787   doi:10.1029/2011GL048733, 2011.

788   Montero-Serrano, J.-C., Frank, N., Tisnérat-Laborde, N., Colin, C., Wu, C., Lin, K., Shen, C., Copard, K.,
789   Orejas, C., Gori, A., De Mol, L., Van Rooij, D., Reverdin, G. and Douville, E.: Decadal changes in the mid-
790   depth water mass dynamic of the Northeastern Atlantic margin (Bay of Biscay), Earth Planet. Sci. Lett., 364,
791   134–144, doi:10.1016/j.epsl.2013.01.012, 2013.

792   Moreno, A., Cacho, I., Canals, M., Prins, M. a., Sánchez-Goñi, M.-F., Grimal, O. J. and Weltje, G. J.: Saharan
793   Dust Transport and High-Latitude Glacial Climatic Variability: The Alboran Sea Record, Quat. Res., 58, 318–
794   328, doi:10.1006/qres.2002.2383, 2002.

795   Moreno, A., Cacho, I., Canals, M., Grimalt, J. O., Sánchez-Goñi, M. F., Shackleton, N. and Sierro, F. J.: Links
796   between marine and atmospheric processes oscillating on a millennial time-scale. A multi-proxy study of the last
797   50,000yr from the Alboran Sea (Western Mediterranean Sea), Quat. Sci. Rev., 24(14-15), 1623–1636,
798   doi:10.1016/j.quascirev.2004.06.018, 2005.

799   Myers, P. G., Haines, K. and Rohling, E. J.: Modeling the paleocirculation of the Mediterranean: The Last
800   Glacial Maximum and the Holocene with emphasis on the formation of sapropel S1, Paleoceanography, 13(6),

586–606, doi:10.1029/98PA02736, 1998.

Ovchinnikov, I. M.: The formation of intermediate water in the Mediterranean, Oceanology, 24, 168–173, 1984.

Overpeck, J. T., Webb, T. and Prentice, I. C.: Quantitative interpretation of fossil pollen spectra: Dissimilarity coefficients and the method of modern analogs, Quat. Res., 23(1), 87–108, doi:10.1016/0033-5894(85)90074-2, 1985.

Paterne, M., Kallel, N., Labeyrie, L., Vautravers, M., Duplessy, J.-C., Rossignol-Strick, M., Cortijo, E., Arnold, M. and Fontugne, M.: Hydrological relationship between the North Atlantic Ocean and the Mediterranean Sea during the past 15-75 kyr, Paleoceanography, 14(5), 626–638, doi:10.1029/1998PA900022, 1999.

Pérez-Folgado, M., Sierro, F. J., Flores, J. A., Cacho, I., Grimalt, J. O., Zahn, R. and Shackleton, N.: Western Mediterranean planktonic foraminifera events and millennial climatic variability during the last 70 kyr, Mar. Micropaleontol., 48(1-2), 49–70, doi:10.1016/S0377-8398(02)00160-3, 2003.

Pinardi, N. and Masetti, E.: Variability of the large scale general circulation of the Mediterranean Sea from observations and modelling: a review, Palaeogeogr. Palaeoclimatol. Palaeoecol., 158(3-4), 153–173, doi:10.1016/S0031-0182(00)00048-1, 2000.

Piotrowski, A. M., Galy, A., Nicholl, J. a. L., Roberts, N. L., Wilson, D. J., Clegg, J. a. and Yu, J.: Reconstructing deglacial North and South Atlantic deep water sourcing using foraminiferal Nd isotopes, Earth Planet. Sci. Lett., 357-358, 289–297, doi:10.1016/j.epsl.2012.09.036, 2012.

Pons-Branchu, E., Douville, E., Roy-Barman, M., Dumont, E., Branchu, P., Thil, F., Frank, N., Bordier, L. and Borst, W.: A geochemical perspective on Parisian urban history based on U–Th dating, laminae counting and yttrium and REE concentrations of recent carbonates in underground aqueducts, Quat. Geochronol., 24, 44–53, doi:10.1016/j.quageo.2014.08.001, 2014.

Prell, W. L.: Stability of low-latitude sea-surface temperatures: an evaluation of the CLIMAP reconstruction with emphasis on the positive SST anomalies. Final report, Providence, RI (USA)., 1985.

Reimer, P. J., Bard, E., Bayliss, A., Beck, J. W., Blackwell, P. G., Bronk Ramsey, C., Grootes, P. M., Guilderson, T. P., Haflidason, H., Hajdas, I., HattŽ, C., Heaton, T. J., Hoffmann, D. L., Hogg, A. G., Hughen, K. A., Kaiser, K. F., Kromer, B., Manning, S. W., Niu, M., Reimer, R. W., Richards, D. A., Scott, E. M., Southon, J. R., Staff, R. A., Turney, C. S. M., & van der Plicht, J. (2013). IntCal13 and Marine13 Radiocarbon Age Calibration Curves 0-50,000 Years cal BP. *Radiocarbon, 55*(4).

Revel, M., Colin, C., Bernasconi, S., Combourieu-Nebout, N., Ducassou, E., Grousset, F. E., Rolland, Y., Migeon, S., Bosch, D., Brunet, P., Zhao, Y. and Mascle, J.: 21,000 Years of Ethiopian African monsoon variability recorded in sediments of the western Nile deep-sea fan, Reg. Environ. Chang., 14(5), 1685–1696, doi:10.1007/s10113-014-0588-x, 2014.

Revel, M., Ducassou, E., Skonieczny, C., Colin, C., Bastian, L., Bosch, D., Migeon, S. and Mascle, J.: 20,000 years of Nile River dynamics and environmental changes in the Nile catchment area as inferred from Nile upper

835   continental slope sediments, Quat. Sci. Rev., 130, 200–221, doi:10.1016/j.quascirev.2015.10.030, 2015.

836   Roberts, N. L., Piotrowski, A. M., McManus, J. F. and Keigwin, L. D.: Synchronous deglacial overturning and
837   water mass source changes., Science, 327(2010), 75–78, doi:10.1126/science.1178068, 2010.

838   Rodrigo-Gámiz, M., Martínez-Ruiz, F., Rampen, S. W., Schouten, S. and Sinninghe Damsté, J. S.: Sea surface
839   temperature variations in the western Mediterranean Sea over the last 20 kyr: A dual-organic proxy (U K′ 37 and
840   LDI) approach, Paleoceanography, 29(2), 87–98, doi:10.1002/2013PA002466, 2014.

841   Rodrigo-Gámiz, M., Martínez-Ruiz, F., Chiaradia, M., Jiménez-Espejo, F. J. and Ariztegui, D.: Radiogenic
842   isotopes for deciphering terrigenous input provenance in the western Mediterranean, Chem. Geol., 410, 237–250,
843   doi:10.1016/j.chemgeo.2015.06.004, 2015.

844   Rogerson, M., Rohling, E. J., Weaver, P. P. E. and Murray, J. W.: Glacial to interglacial changes in the settling
845   depth of the Mediterranean Outflow plume, Paleoceanography, 20(3), doi:10.1029/2004PA001106, 2005.

846   Rogerson, M., Rohling, E. J. and Weaver, P. P. E.: Promotion of meridional overturning by Mediterranean-
847   derived salt during the last deglaciation, Paleoceanography, 21(4), 1–8, doi:10.1029/2006PA001306, 2006.

848   Rogerson, M., Cacho, I., Jimenez-Espejo, F., Reguera, M. I., Sierro, F. J., Martinez-Ruiz, F., Frigola, J. and
849   Canals, M.: A dynamic explanation for the origin of the western Mediterranean organic-rich layers,
850   Geochemistry, Geophys. Geosystems, 9(7), n/a–n/a, doi:10.1029/2007GC001936, 2008.

851   Rohling, E. J.: Review and new aspects concerning the formation of eastern Mediterranean sapropels, Mar.
852   Geol., 122(1-2), 1–28, doi:10.1016/0025-3227(94)90202-X, 1994.

853   Rohling, E. J., Jorissen, F. J. and De stigter, H. C.: 200 Year interruption of Holocene sapropel formation in the
854   Adriatic Sea, J. Micropalaeontology, 16(2), 97–108, doi:10.1144/jm.16.2.97, 1997.

855   Rohling, E. J., Mayewski, P. a, Abu-Zied, R. H., Casford, J. S. L. and Hayes, A.: Holocene atmosphere-ocean
856   interactions: records from Greenland and the Aegean Sea, Clim. Dyn., 18(7), 587–593, doi:10.1007/s00382-001-
857   0194-8, 2002.

858   Rohling, E. J., Sprovieri, M., Cane, T., Casford, J. S. ., Cooke, S., Bouloubassi, I., Emeis, K. C., Schiebel, R.,
859   Rogerson, M., Hayes, A., Jorissen, F. . and Kroon, D.: Reconstructing past planktic foraminiferal habitats using
860   stable isotope data: a case history for Mediterranean sapropel S5, Mar. Micropaleontol., 50(1-2), 89–123,
861   doi:10.1016/S0377-8398(03)00068-9, 2004.

862   Rohling, E. J., Marino, G. and Grant, K. M.: Mediterranean climate and oceanography, and the periodic
863   development of anoxic events (sapropels), Earth-Science Rev., 143, 62–97, doi:10.1016/j.earscirev.2015.01.008,
864   2015.

865   Rossignol-Strick, M., Nesteroff, W., Olive, P. and Vergnaud-Grazzini, C.: After the deluge: Mediterranean
866   stagnation and sapropel formation, Nature, 295(5845), 105–110, doi:10.1038/295105a0, 1982.

867   Sammari, C., Millot, C., Taupier-Letage, I., Stefani, A. and Brahim, M.: Hydrological characteristics in the

868 Tunisia–Sardinia–Sicily area during spring 1995, Deep Sea Res. Part I Oceanogr. Res. Pap., 46(10), 1671–1703,
869 doi:10.1016/S0967-0637(99)00026-6, 1999.

870 Sarmiento, J. L., Herbert, T. and Toggweiler, J. R.: Mediterranean nutrient balance and episodes of anoxia,
871 Global Biogeochem. Cycles, 2(4), 427–444, doi:10.1029/GB002i004p00427, 1988.

872

873 Sánchez-Goñi, M., Cacho, I., Turon, J. L., Guiot, J., Sierro, F. J., Peypouquet, J., Grimalt, J. O. and Shackleton,
874 N. J.: Synchroneity between marine and terrestrial responses to millennial scale climatic variability during the
875 last glacial period in the Mediterranean region, Clim. Dyn., 19(1), 95–105, doi:10.1007/s00382-001-0212-x,
876 2002.

877 Sarnthein, M., Tetzlaff, G., Koopmann, B., Wolter, K. and Pflaumann, U.: Glacial and interglacial wind regimes
878 over the eastern subtropical Atlantic and North-West Africa, Nature, 293, 193–196, doi:10.1038/293193a0,
879 1981.

880 Scheuvens, D., Schütz, L., Kandler, K., Ebert, M. and Weinbruch, S.: Bulk composition of northern African dust
881 and   its   source   sediments   —   A   compilation,   Earth-Science   Rev.,   116,   170–194,
882 doi:10.1016/j.earscirev.2012.08.005, 2013.

883 Schmiedl, G., Kuhnt, T., Ehrmann, W., Emeis, K. C., Hamann, Y., Kotthoff, U., Dulski, P. and Pross, J.:
884 Climatic forcing of eastern Mediterranean deep-water formation and benthic ecosystems during the past 22 000
885 years, Quat. Sci. Rev., 29(23-24), 3006–3020, doi:10.1016/j.quascirev.2010.07.002, 2010.

886 Schönfeld, J. and Zahn, R.: Late Glacial to Holocene history of the Mediterranean outflow. Evidence from
887 benthic foraminiferal assemblages and stable isotopes at the Portuguese margin, Palaeogeogr. Palaeoclimatol.
888 Palaeoecol., 159(1-2), 85–111, doi:10.1016/S0031-0182(00)00035-3, 2000.

889 Schott, F., Visbeck, M., Send, U., Fischer, J., Stramma, L. and Desaubies, Y.: Observations of Deep Convection
890 in the Gulf of Lions, Northern Mediterranean, during the Winter of 1991/92, J. Phys. Oceanogr., 26(4), 505–524,
891 doi:10.1175/1520-0485(1996)026<0505:OODCIT>2.0.CO;2, 1996.

892 Schroeder, K., Millot, C., Bengara, L., Ben Ismail, S., Bensi, M., Borghini, M., Budillon, G., Cardin, V.,
893 Coppola, L., Curtil, C., Drago, A., El Moumni, B., Font, J., Fuda, J. L., García-Lafuente, J., Gasparini, G. P.,
894 Kontoyiannis, H., Lefevre, D., Puig, P., Raimbault, P., Rougier, G., Salat, J., Sammari, C., Sánchez Garrido, J.
895 C., Sanchez-Roman, A., Sparnocchia, S., Tamburini, C., Taupier-Letage, I., Theocharis, A., Vargas-Yáñez, M.
896 and Vetrano, A.: Long-term monitoring programme of the hydrological variability in the Mediterranean Sea: a
897 first overview of the HYDROCHANGES network, Ocean Sci., 9(2), 301–324, doi:10.5194/os-9-301-2013,
898 2013.

899 Scrivner, A. E., Vance, D. and Rohling, E. J.: New neodymium isotope data quantify Nile involvement in
900 Mediterranean anoxic episodes, Geology, 32(7), 565, doi:10.1130/G20419.1, 2004.

901 Shanahan, T. M., McKay, N. P., Hughen, K. A., Overpeck, J. T., Otto-Bliesner, B., Heil, C. W., King, J., Scholz,
902 C. A. and Peck, J.: The time-transgressive termination of the African Humid Period, Nat. Geosci., 8(2), 140–144,

903   doi:10.1038/ngeo2329, 2015.

904   Siani, G., Paterne, M., Arnold, M., Bard, E., Metivier, B., Tisnerat, N. and Bassinot, F.: Radiocarbon reservoir
905   ages in the Mediterranean Sea and Black Sea, Radiocarbon, 42(2), 271–280 [online] Available from: <Go to
906   ISI>://000089971000010, 2000.

907   Siani, G., Paterne, M., Michel, E., Sulpizio, R., Sbrana, A., Arnold, M. and Haddad, G.: Mediterranean Sea
908   surface radiocarbon reservoir age changes since the last glacial maximum., Science (80-.)., 294(5548), 1917–
909   1920, doi:10.1126/science.1063649, 2001.

910   Siani, G., Sulpizio, R., Paterne, M. and Sbrana, A.: Tephrostratigraphy study for the last 18,000 C years in a
911   deep-sea sediment sequence for the South Adriatic, Quat. Sci. Rev., 23(23-24), 2485–2500,
912   doi:10.1016/j.quascirev.2004.06.004, 2004.

913   Siani, G., Magny, M., Paterne, M., Debret, M., Fontugne, M. (2013) - Paleohydrology reconstruction and
914   Holocene climate variability in the South Adriatic Sea. *Climate of the Past,* 9, 499-515.

915   Sierro, F. J., Hodell, D. A., Curtis, J. H., Flores, J. A., Reguera, I., Colmenero-Hidalgo, E., Bárcena, M. A.,
916   Grimalt, J. O., Cacho, I., Frigola, J. and Canals, M.: Impact of iceberg melting on Mediterranean thermohaline
917   circulation during Heinrich events, Paleoceanography, 20(2), n/a–n/a, doi:10.1029/2004PA001051, 2005.

918   Sparnocchia, S., Gasparini, G. P., Astraldi, M., Borghini, M. and Pistek, P.: Dynamics and mixing of the Eastern
919   Mediterranean outflow in the Tyrrhenian basin, J. Mar. Syst., 20(1-4), 301–317, doi:10.1016/S0924-
920   7963(98)00088-8, 1999.

921   Spivack, A. J. and Wasserburg, G. J.: Neodymium isotopic composition of the Mediterranean outflow and the
922   eastern North Atlantic, Geochim. Cosmochim. Acta, 52(12), 2767–2773, doi:10.1016/0016-7037(88)90144-5,
923   1988.

924   Stratford, K., Williams, R. G. and Myers, P. G.: Impact of the circulation on Sapropel Formation in the eastern
925   Mediterranean, Global Biogeochem. Cycles, 14(2), 683–695, doi:10.1029/1999GB001157, 2000.

926   Struiver, M., Reimer, P. J. and Reimer, R.: CALIB 7.0, Radiocarb. Calibration Progr., 2005.

927   Tachikawa, K., Roy-Barman, M., Michard, A., Thouron, D., Yeghicheyan, D. and Jeandel, C.: Neodymium
928   isotopes in the Mediterranean Sea: comparison between seawater and sediment signals, Geochim. Cosmochim.
929   Acta, 68(14), 3095–3106, doi:10.1016/j.gca.2004.01.024, 2004.

930   Tachikawa, K., Piotrowski, A. M. and Bayon, G.: Neodymium associated with foraminiferal carbonate as a
931   recorder of seawater isotopic signatures, Quat. Sci. Rev., 88, 1–13, doi:10.1016/j.quascirev.2013.12.027, 2014.

932   Tanaka, T., Togashi, S., Kamioka, H., Amakawa, H., Kagami, H., Hamamoto, T., Yuhara, M., Orihashi, Y.,
933   Yoneda, S., Shimizu, H., Kunimaru, T., Takahashi, K., Yanagi, T., Nakano, T., Fujimaki, H., Shinjo, R.,
934   Asahara, Y., Tanimizu, M. and Dragusanu, C.: JNdi-1: a neodymium isotopic reference in consistency with
935   LaJolla neodymium, Chem. Geol., 168(3-4), 279–281, doi:10.1016/S0009-2541(00)00198-4, 2000.

936   Tachikawa, K., Vidal, L., Cornuault, M., Garcia, M., Pothin, A., Sonzogni, C., Bard, E., Menot, G. and Revel,
937   M.: Eastern Mediterranean Sea circulation inferred from the conditions of S1 sapropel deposition, Clim. Past,
938   11(6), 855–867, doi:10.5194/cp-11-855-2015, 2015.

939   Taviani, M., Angeletti, L., Canese, S., Cannas, R., Cardone, F., Cau, A., Cau, A. B., Follesa, M. C., Marchese,
940   F., Montagna, P. and Tessarolo, C.: The "Sardinian cold-water coral province" in the context of the
941   Mediterranean coral ecosystems, Deep Sea Res. Part II Top. Stud. Oceanogr., doi:10.1016/j.dsr2.2015.12.008,
942   2015.

943   Thunell, R. C. and Williams, D. F.: Glacial–Holocene salinity changes in the Mediterranean Sea: hydrographic
944   and depositional effects, Nature, 338(6215), 493–496, doi:10.1038/338493a0, 1989.

945   Toucanne, S., Jouet, G., Ducassou, E., Bassetti, M. A., Dennielou, B., Angue Minto'o, C. M., Lahmi, M.,
946   Touyet, N., Charlier, K., Lericolais, G. and Mulder, T.: A 130,000-year record of Levantine Intermediate Water
947   flow variability in the Corsica Trough, western Mediterranean Sea, Quat. Sci. Rev., 33, 55–73,
948   doi:10.1016/j.quascirev.2011.11.020, 2012.

949   Vance, D., Scrivner, A. E. and Beney, P.: The use of foraminifera as a record of the past neodymium isotope
950   composition of seawater, Paleoceanography, 19(2), PA2009, doi:10.1029/2003PA000957, 2004.

951   van de Flierdt, T., Robinson, L. F. and Adkins, J. F.: Deep-sea coral aragonite as a recorder for the neodymium
952   isotopic   composition   of   seawater,   Geochim.   Cosmochim.   Acta,   74(21),   6014–6032,
953   doi:10.1016/j.gca.2010.08.001, 2010.

954   Voelker, A. H. L., Lebreiro, S. M., Schönfeld, J., Cacho, I., Erlenkeuser, H. and Abrantes, F.: Mediterranean
955   outflow strengthening during northern hemisphere coolings: A salt source for the glacial Atlantic?, Earth Planet.
956   Sci. Lett., 245, 39–55, doi:10.1016/j.epsl.2006.03.014, 2006.

957   Weaver, A. J., Saenko, O. a., Clark, P. U. and Mitrovica, J. X.: Meltwater Pulse 1A from Antarctica as a Trigger
958   of the Bolling-Allerod Warm Interval, Science (80-.)., 299(5613), 1709–1713, doi:10.1126/science.1081002,
959   2003.

960   Weldeab, S., Emeis, K.-C., Hemleben, C. and Siebel, W.: Provenance of lithogenic surface sediments and
961   pathways of riverine suspended matter in the Eastern Mediterranean Sea: evidence from 143Nd/144Nd and
962   87Sr/86Sr ratios, Chem. Geol., 186(1-2), 139–149, doi:10.1016/S0009-2541(01)00415-6, 2002.

963   Weldeab, S., Menke, V. and Schmiedl, G.: The pace of East African monsson evolution during the Holocene,
964   Geophys. Res. Lett., 41, 1724–1731, doi:10.1002/2014GL059361.Received, 2014.

965   Wienberg, C., Frank, N., Mertens, K. N., Stuut, J.-B. W., Marchant, M., Fietzke, J., Mienis, F. and Hebbeln, D.:
966   Glacial cold-water coral growth in the Gulf of Cádiz: Implications of increased palaeo-productivity, Earth
967   Planet. Sci. Lett., 298(3-4), 405–416, doi:10.1016/j.epsl.2010.08.017, 2010.

968   Wu, Q., Colin, C., Liu, Z., Thil, F., Dubois-Dauphin, Q., Frank, N., Tachikawa, K., Bordier, L. and Douville, E.:
969   Neodymium isotopic composition in foraminifera and authigenic phases of the South China Sea sediments:

970 Implications for the hydrology of the North Pacific Ocean over the past 25 kyr, Geochemistry, Geophys.
971 Geosystems, 16(11), 3883–3904, doi:10.1002/2015GC005871, 2015.

972 **Table captions**

973

974 **Table 1**. U-series ages and εNd values obtained for cold-water coral samples collected from sediment core RECORD 23
975 (Sardinia Channel).

976

977 **Table 2**. εNd values obtained for cold-water corals from the southern Alboran Sea. The AMS ^{14}C ages published by Fink et
978 al. (2013) are also reported as Median probability age (ka BP).

979

980 **Table 3**. AMS ^{14}C ages of samples of the planktonic foraminifer *G. bulloides* from 'off-mound' sediment core SU92-33. The
981 AMS ^{14}C ages were corrected for ^{13}C and a mean reservoir age of 400 yrs, and were converted into calendar years using the
982 INTCAL13 calibration data set (Reimer et al., 2013) and the CALIB 7.0 program (Struiver et al., 2005).

983

984 **Table 4**. Multiproxy data obtained for the upper 2.1 m of sediment core SU92-33 (Balearic Sea). Stable oxygen and carbon
985 isotopes were measured on benthic (*C. pachyderma*) and planktonic (*G. bulloides*) foraminifera; εNd values were obtained on
986 mixed planktonic foraminifera samples. The age results from a combination of 7 AMS-^{14}C age measurements for the upper
987 1.2 m of the core and by a linear interpolation between these ages as well as the $\delta^{18}O$ variations of the planktonic
988 foraminifera *G. bulloides.*

989

990 **Figure captions**

991

992 **Figure 1**. Map of the western Mediterranean Sea showing the locations of samples investigated in this study. Yellow dot
993 indicates the sampling location of the sediment core from the Balearic Sea (SU92-33); yellow stars indicate the locations of
994 the CWC-bearing cores from the Sardinia Channel (RECORD 23) and the southern Alboran Sea (for further details on the
995 CWC from the Alboran Sea refer also to Fink et al., 2013). The cores discussed in this paper (Gulf of Cádiz: IODP site
996 U1387, Balearic Sea: MD09-2343, northern Tyrrhenian Sea: MD01-2472, Adriatic Sea: MD90-917) are indicated by black
997 dots, and seawater stations are marked by open squares. Arrows represent the main oceanographic currents. The black line
998 shows the general trajectory of the Modified Atlantic Water (MAW) flowing at the surface from the Atlantic Ocean toward
999 the western and eastern Mediterranean. The orange line represents the Levantine Intermediate Water (LIW) originating from
1000 the eastern basin. The black dashed line shows the trajectory of the Western Mediterranean Deep Water (WMDW) flowing
1001 from the Gulf of Lions toward the Strait of Gibraltar.

1002

1003 **Figure 2**. (a) Sea Surface Temperature (SST) records of cores SU92-33 (red line) and MD90-917 (green line; Siani et al.,
1004 2004), (b) $\delta^{18}O$ record obtained on planktonic foraminifer *G. bulloides* for core SU92-33, (c) $\delta^{18}O$ record obtained on benthic
1005 foraminifer *C. pachyderma* for core SU92-33, (d) $\delta^{13}C$ record obtained on benthic foraminifer *C. pachyderma* for core SU92-
1006 33. LGM: Last Glacial Maximum; HS1: Heinrich Stadial 1; B-A: Bølling-Allerød; YD: Younger Dryas. Black triangles
1007 indicate AMS ^{14}C age control points.

1008

1009 **Figure 3**. (a) Sea Surface Temperature (SST) record of core SU92-33 (red line), (b) εNd records obtained on mixed
1010 planktonic foraminifers from core SU92-33 (open circles) and from cold-water coral fragments collected in the Alboran Sea
1011 (red squares), (c) εNd values of cold-water corals from core RECORD 23 (Sardinia Channel).

1012

Figure 4. (a) δ^{13}C records obtained on benthic foraminifer *C. pachyderma* for cores SU92-33 (red line) and MD99-2343 (blue line; Sierro et al., 2005). (b) εNd records obtained on mixed planktonic foraminifers from core SU92-33 (open circles) and from cold-water coral fragments collected in the Alboran Sea (red squares). Modern εNd values for LIW (orange dashed line) and WMDW (blue dashed line) are also reported for comparison. (c) εNd values obtained for planktonic foraminifera with Fe-Mn coatings at sites 300G (36°21.532' N, 1°47.507' W; 1860 m; open dots) and 304G (36°19.873' N, 1°31.631' W; 2382 m; black dots) in Alboran Sea (Jimenez-Espejo et al., 2015). (d) UP10 fraction (>10 μm) from core MD99-2343 (Frigola et al., 2008). (e) Sortable silt mean grain-size of core MD01-2472 (Toucanne et al., 2012). (f) Ln Zr/Al ratio at IODP site U1387 (36°48.3' N 7°43.1' W; 559 m) (Bahr et al., 2015).

Figure 5. (a) δ^{18}O record obtained on planktonic foraminifer *G. bulloides* for core SU92-33, (b) δ^{13}C records obtained on benthic foraminifer *C. pachyderma* for core SU92-33, (c) εNd values of cold-water corals from core RECORD 23 (Sardinia Channel), (d) εNd values records obtained on mixed planktonic foraminifera from core SU92-33 (open circles) and from cold-water coral fragments collected in the Alboran Sea (red squares), (e) εNd values obtained on terrigenous fraction of MS27PT located close the Nile River mouth in the eastern Mediterranean basin (Revel et al., 2015).
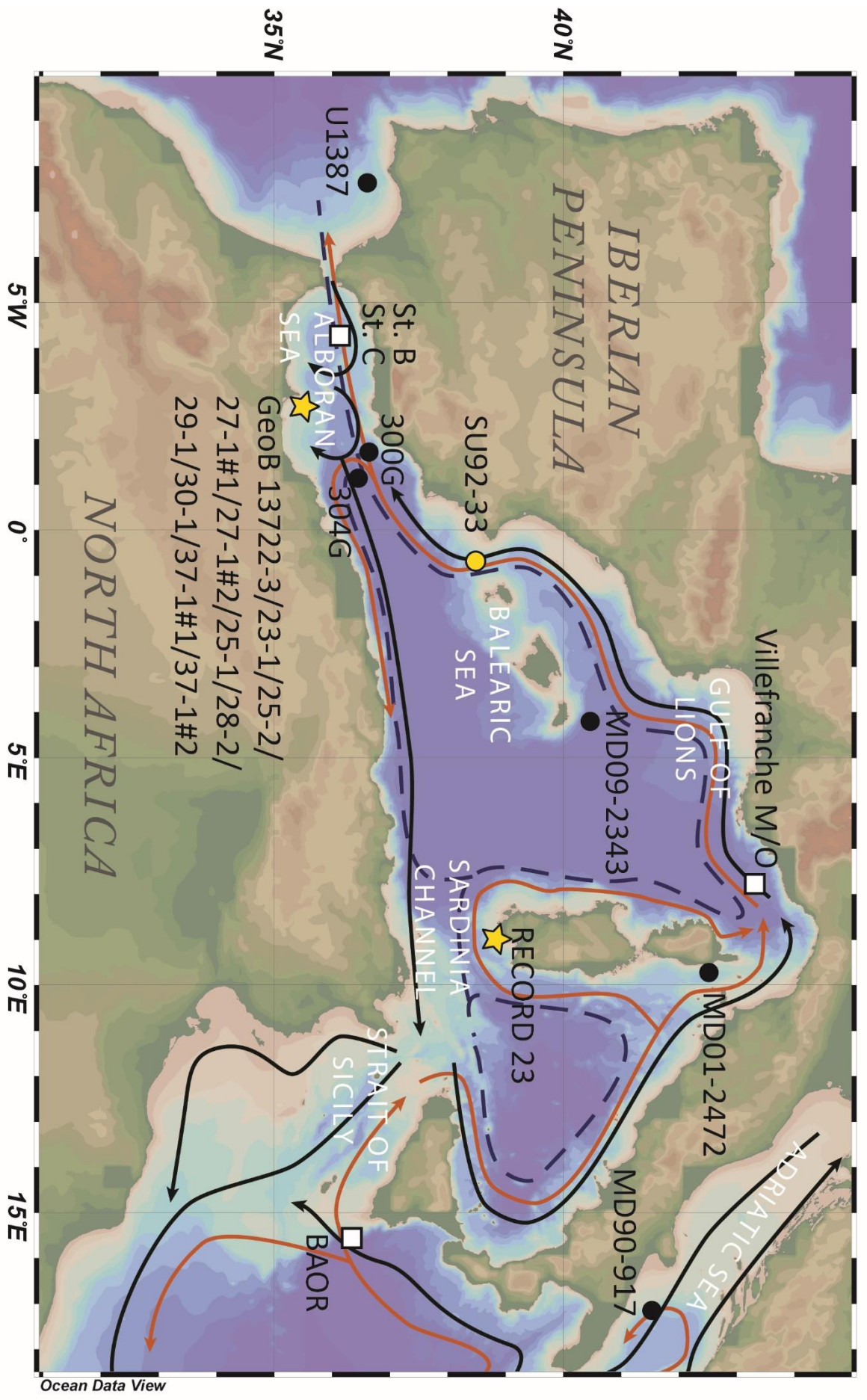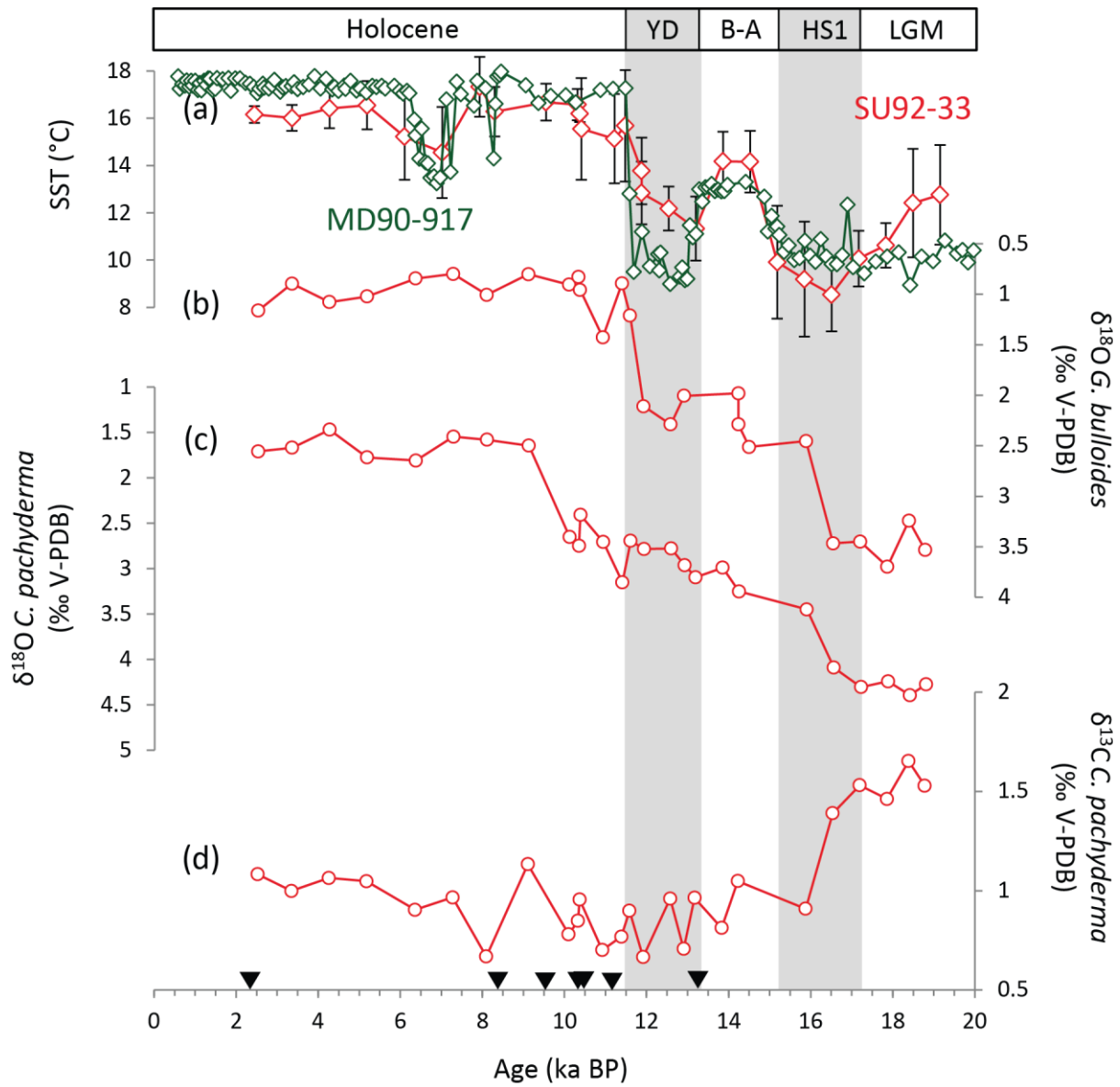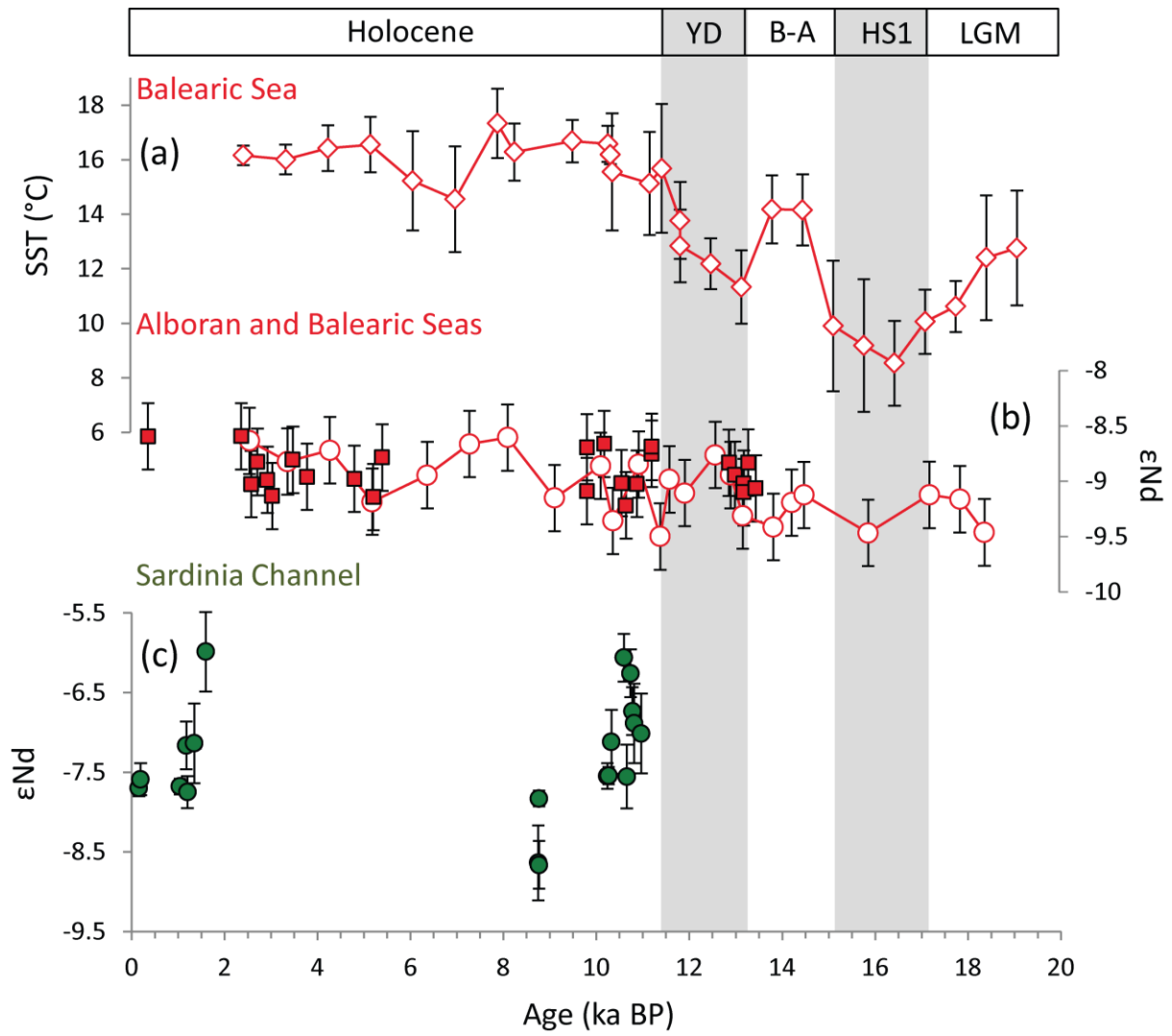
Figure 2

Figure 3

Figure 4

Figure 5

Table 1
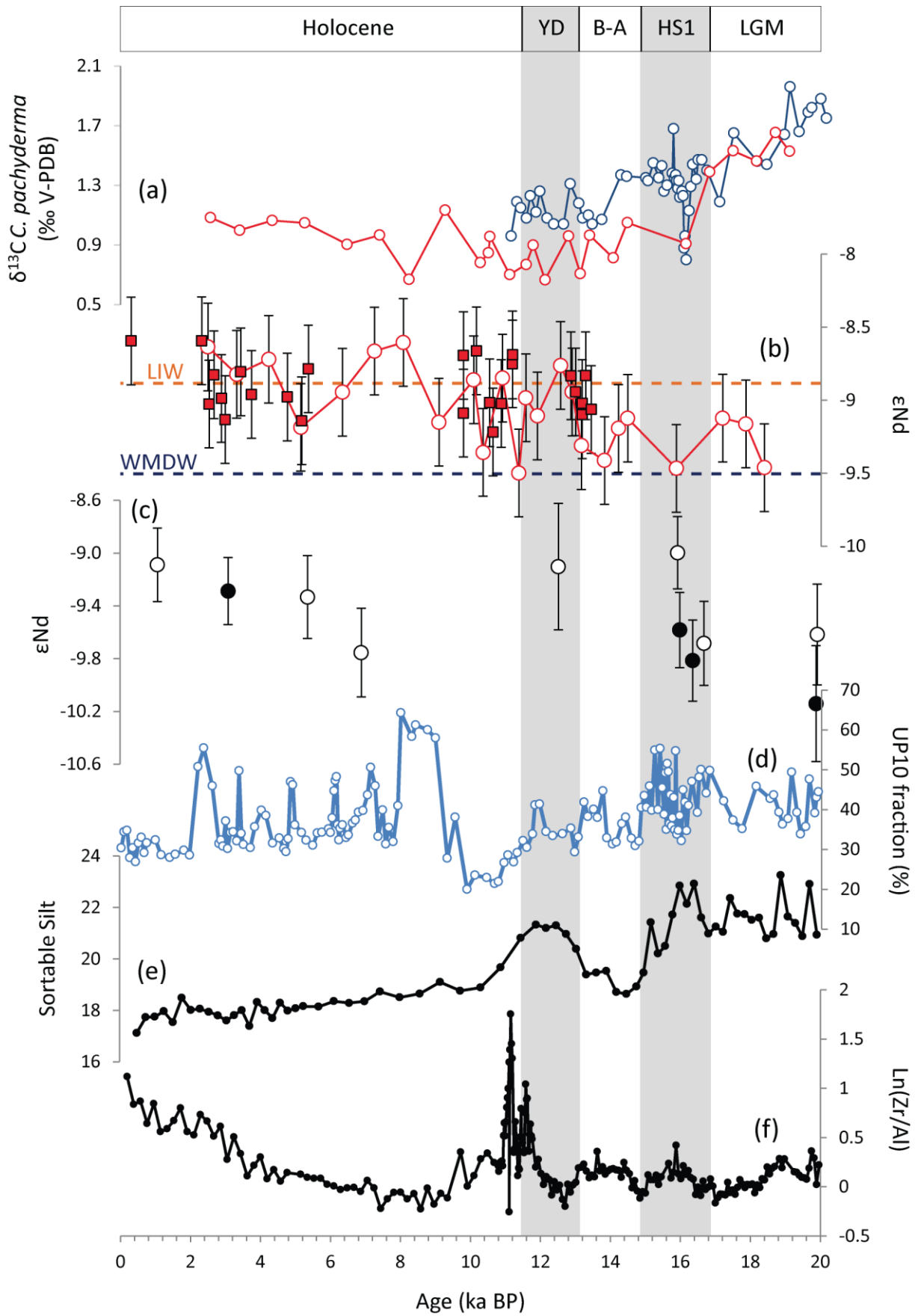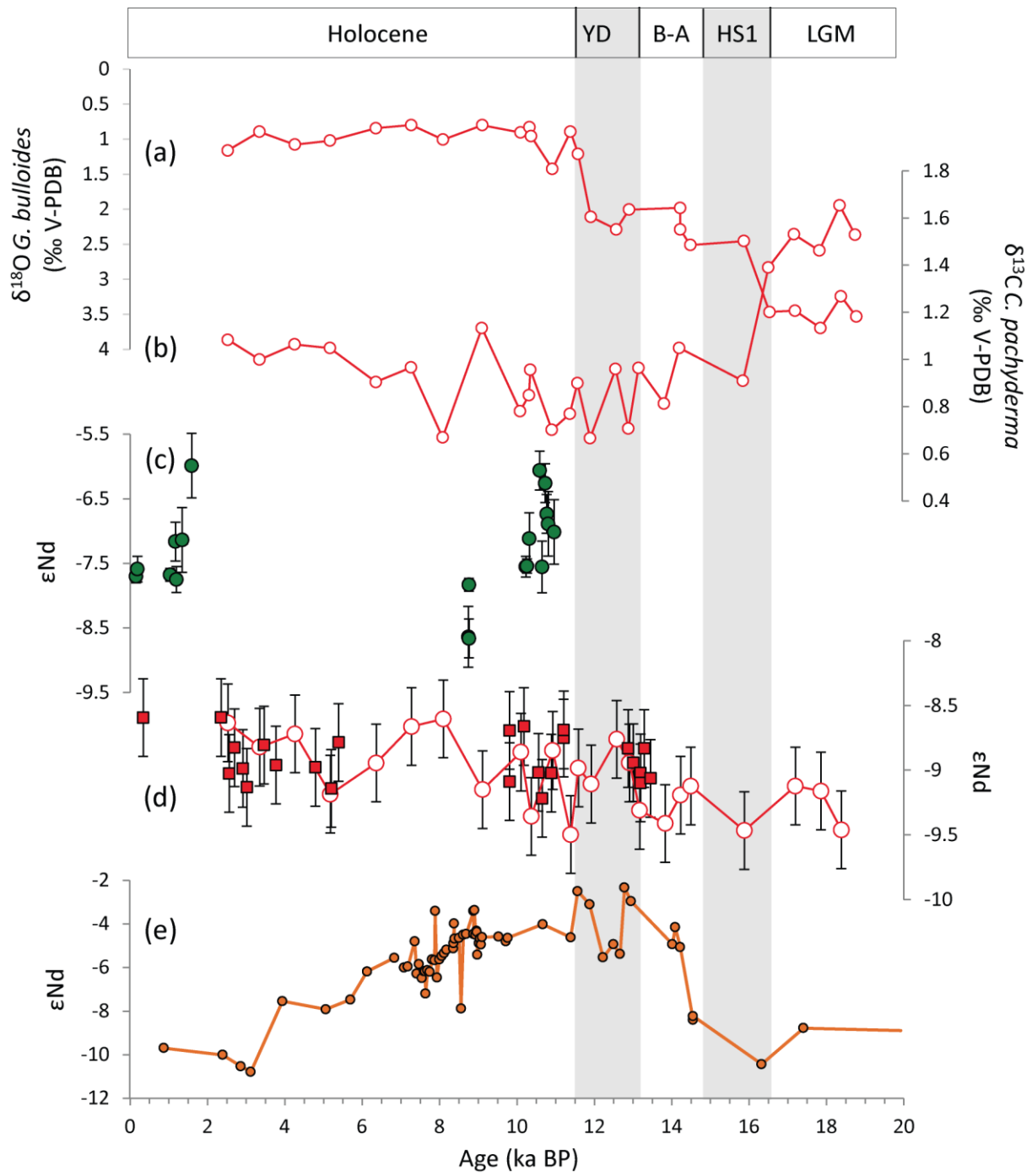
Sample ID	Depth in core (cm)	Corals species	^{238}U (µg/g)	^{232}Th (ng/g)	$\delta^{234}U_m$ (‰)	$^{230}Th/^{238}U$	$^{230}Th/^{232}Th$	Age (ka BP)	$\delta^{234}U_{(0)}$ (‰)	$^{143}Nd/^{144}Nd$	εNd
RECORD_23_V	0-3,5	Madrepora oculata	3.31 ±0.005	0.68 ±0.014	151.85 ±1.7	0.00163 ±0.00011	25 ±1.7	0.091 ±0.011	151.92 ±1.7	0.512243 ±0.000005	-7.70 ±0.10
RECORD_23_V	3-7	Madrepora oculata	3.23 ±0.002	0.52 ±0.001	147.11 ±0.6	0.00199 ±0.00006	38 ±1.1	0.127 ±0.006	147.19 ±0.6	0.512249 ±0.000010	-7.59 ±0.20
RECORD_23_V	7-10	Madrepora oculata	3.99 ±0.007	0.25 ±0.002	147.52 ±1.7	0.01227 ±0.00022	640 ±11.6	1.110 ±0.023	148.01 ±1.7	0.512244 ±0.000015	-7.68 ±0.30
RECORD_23_V	8-10	Madrepora oculata	3.79 ±0.005	0.41 ±0.001	147.77 ±0.7	0.01253 ±0.00007	350 ±2.0	1.135 ±0.008	148.27 ±0.7	0.512271 ±0.000010	-7.16 ±0.20
RECORD_23_IV	6-9	Madrepora oculata	4.06 ±0.006	0.35 ±0.001	148.47 ±1.2	0.01366 ±0.00011	480 ±3.8	1.243 ±0.012	149.02 ±1.2	0.512241 ±0.000010	-7.75 ±0.20
RECORD_23_IV	27-30	Madrepora oculata	4.06 ±0.003	1.09 ±0.001	146.91 ±1.3	0.01405 ±0.00013	159 ±1.4	1.283 ±0.014	147.47 ±1.3	0.512272 ±0.000026	-7.14 ±0.50
RECORD_23_IV	37-40	Madrepora oculata	3.52 ±0.005	0.08 ±0.000	148.25 ±1.1	0.01663 ±0.00012	2308 ±16.4	1.529 ±0.013	148.92 ±1.1	0.512331 ±0.000026	-5.99 ±0.50
RECORD_23_III	55-57	Madrepora oculata	3.63 ±0.002	0.27 ±0.000	145.30 ±0.7	0.08832 ±0.00020	3530 ±8.1	8.685 ±0.027	148.93 ±0.8	0.512195 ±0.000026	-8.64 ±0.50
RECORD_23_III	58-61	Madrepora oculata	4.24 ±0.004	0.36 ±0.001	146.71 ±1.2	0.08859 ±0.00037	3336 ±14.0	8.702 ±0.048	150.39 ±1.2	0.512237 ±0.000010	-7.83 ±0.20
RECORD_23_III	63-66	Lophelia pertusa	4.15 ±0.005	0.42 ±0.002	147.19 ±0.8	0.08863 ±0.00054	2783 ±17.1	8.703 ±0.063	150.89 ±0.9	0.512194 ±0.000015	-8.66 ±0.30
RECORD_23_I	0-2	Lophelia pertusa	3.35 ±0.002	0.37 ±0.000	147.02 ±0.7	0.10283 ±0.00018	2788 ±4.8	10.173 ±0.025	151.34 ±0.7	0.512251 ±0.000010	-7.55 ±0.20
RECORD_23_I	62-65	Lophelia pertusa	3.27 ±0.003	0.39 ±0.002	144.75 ±1.2	0.10289 ±0.00061	2721 ±16.1	10.201 ±0.075	149.01 ±1.2	0.512251 ±0.000010	-7.54 ±0.20
RECORD_23_II	50-52	Lophelia pertusa	2.92 ±0.003	0.92 ±0.003	145.39 ±1.6	0.10351 ±0.00061	1046 ±6.2	10.260 ±0.079	149.69 ±1.6	0.512273 ±0.000021	-7.12 ±0.40
RECORD_23_I	12-14	Lophelia pertusa	3.07 ±0.002	0.49 ±0.000	145.22 ±0.7	0.10609 ±0.00023	1971 ±4.3	10.531 ±0.031	149.64 ±0.7	0.512327 ±0.000015	-6.06 ±0.30
RECORD_23_I	5-7	Lophelia pertusa	3.50 ±0.002	0.42 ±0.000	146.35 ±0.9	0.10677 ±0.00016	2654 ±4.0	10.591 ±0.025	150.82 ±0.9	0.512251 ±0.000015	-7.55 ±0.40
RECORD_23_II	94-98	Lophelia pertusa	3.14 ±0.003	0.62 ±0.002	146.42 ±1.0	0.10755 ±0.00047	1737 ±7.6	10.672 ±0.059	150.94 ±1.0	0.512317 ±0.000015	-6.26 ±0.30
RECORD_23_II	15-17	Lophelia pertusa	3.40 ±0.003	0.46 ±0.000	146.01 ±0.9	0.10790 ±0.00021	2409 ±4.6	10.713 ±0.031	150.53 ±0.9	0.512293 ±0.000015	-6.73 ±0.30
RECORD_23_II	96-100	Lophelia pertusa	3.61 ±0.004	0.35 ±0.001	145.50 ±0.8	0.10821 ±0.00044	3579 ±14.7	10.750 ±0.055	150.02 ±0.8	0.512285 ±0.000026	-6.89 ±0.50
RECORD_23_II	93-95	Lophelia pertusa	3.19 ±0.003	0.24 ±0.000	143.33 ±0.8	0.10947 ±0.00032	4381 ±12.7	10.904 ±0.042	147.85 ±0.9	0.512279 ±0.000026	-7.01 ±0.50

Sample ID	Core depth (cm)	Species	Water Depth (m)	Median probability age (ka BP)	^{143}Nd/^{144}Nd	εNd
GeoB 13727-1#1	Surface	*Lophelia pertusa*	363	0.339	0.512198 ±0.000015	-8.59 ±0.30
GeoB 13727-1#2	Surface	*Madrepora oculata*	353	2.351	0.512198 ±0.000015	-8.59 ±0.30
GeoB 13730-1	6	*Lophelia pertusa*	338	2.563	0.512175 ±0.000015	-9.03 ±0.30
GeoB 13728-1	Bulk (0-15)	*Lophelia pertusa*	343	2.698	0.512185 ±0.000015	-8.83 ±0.30
GeoB 13728-2	2	*Lophelia pertusa*	343	2.913	0.512177 ±0.000015	-8.99 ±0.30
GeoB 13722-3	Bulk (0-15)	*Madrepora oculata*	280	3.018	0.512170 ±0.000015	-9.13 ±0.30
GeoB 13722-3	Bulk (15-30)	*Madrepora oculata*	280	3.463	0.512186 ±0.000015	-8.81 ±0.30
GeoB 13735-1	Bulk (0-15)	*Madrepora oculata*	280	3.770	0.512179 ±0.000015	-8.96 ±0.30
GeoB 13723-1	Bulk (0-8)	*Madrepora oculata*	291	4.790	0.512178 ±0.000015	-8.98 ±0.30
GeoB 13725-2	Surface	*Madrepora oculata*	355	5.201	0.512169 ±0.000015	-9.14 ±0.30
GeoB 13723-1	Bulk (8-20)	*Madrepora oculata*	291	5.390	0.512187 ±0.000015	-8.79 ±0.30
GeoB 13729-1	2.5	*Lophelia pertusa*	442	9.810	0.512172 ±0.000015	-9.09 ±0.30
GeoB 13729-1	2.5	*Lophelia pertusa*	442	9.810	0.512193 ±0.000015	-8.69 ±0.30
GeoB 13729-1	49	*Lophelia pertusa*	442	10.181	0.512194 ±0.000015	-8.66 ±0.30
GeoB 13730-1	102	*Lophelia pertusa*	338	10.556	0.512176 ±0.000015	-9.02 ±0.30
GeoB 13730-1	194	*Lophelia pertusa*	338	10.652	0.512165 ±0.000015	-9.22 ±0.30
GeoB 13729-1	315	*Lophelia pertusa*	442	10.889	0.512176 ±0.000015	-9.02 ±0.30
GeoB 13729-1	375	*Lophelia pertusa*	442	11.206	0.512189 ±0.000015	-8.75 ±0.30
GeoB 13730-1	298	*Lophelia pertusa*	338	11.208	0.512193 ±0.000015	-8.69 ±0.30
GeoB 13728-2	191	*Lophelia pertusa*	343	12.874	0.512185 ±0.000015	-8.83 ±0.30
GeoB 13737-1#2	Surface	*Lophelia pertusa*	297	13.005	0.512180 ±0.000015	-8.94 ±0.30
GeoB 13728-2	295	*Lophelia pertusa*	364	13.194	0.512176 ±0.000015	-9.02 ±0.30
GeoB 13728-2	295	*Lophelia pertusa*	364	13.194	0.512171 ±0.000015	-9.10 ±0.30
GeoB 13730-1	427	*Lophelia pertusa*	338	13.291	0.512185 ±0.000015	-8.83 ±0.30
GeoB 13737-1#1	Surface	*Lophelia pertusa*	299	13.452	0.512174 ±0.000015	-9.06 ±0.30

Table 2

Core	Depth in core (cm)	^{14}C-age (years)	±1σ (years)	Median probability age (ka BP)
SU92-33	0	2770	70	2437
SU92-33	64	7870	90	8280
SU92-33	70	8670	80	9528
SU92-33	74	9510	100	10295
SU92-33	84	9610	90	10389
SU92-33	90	10180	100	11192
SU92-33	120	11710	110	13172

Table 3

Depth in core (cm)	Age (ka BP)	δ¹³C C. pachyderma (‰ VPDB)	δ¹⁸O C. pachyderma (‰ VPDB)	δ¹³C G. bulloides (‰ VPDB)	δ¹⁸O G. bulloides (‰ VPDB)	¹⁴³Nd/¹⁴⁴Nd	εNd	
1	2.53	1.08	1.71	-0.6	1.16	0.512195 ±0.000015	-8.64	±0.30
10	3.35	1.00	1.67	-0.82	0.90	0.512186 ±0.000015	-8.82	±0.30
19.5	4.26	1.06	1.47	-0.55	1.08	0.512191 ±0.000015	-8.72	±0.30
29.5	5.18	1.05	1.78	-0.55	1.02	0.512167 ±0.000015	-9.19	±0.30
42.5	6.36	0.90	1.81	-0.91	0.84	0.512179 ±0.000015	-8.95	±0.30
52.5	7.28	0.97	1.55	-0.80	0.80	0.512194 ±0.000015	-8.66	±0.30
61.5	8.10	0.67	1.58	-0.95	1.01	0.512197 ±0.000015	-8.61	±0.30
67.5	9.11	1.13	1.65	-1.07	0.80	0.512169 ±0.000015	-9.15	±0.30
72.5	10.10	0.78	2.65	-1.27	0.91	0.512184 ±0.000015	-8.86	±0.30
77.5	10.33	0.85	2.75	-1.10	0.83	-	-	-
81.5	10.37	0.96	2.41	-1.21	0.96	0.512158 ±0.000015	-9.36	±0.30
87.5	10.92	0.70	2.71	-0.11	1.43	0.512184 ±0.000015	-8.85	±0.30
92.5	11.39	0.77	3.15	-1.00	0.89	0.512151 ±0.000015	-9.50	±0.30
95.5	11.59	0.90	2.69	-1.14	1.21	0.512178 ±0.000015	-8.98	±0.30
100.5	11.92	0.67	2.78	-0.44	2.11	0.512171 ±0.000015	-9.11	±0.30
110.5	12.58	0.96	2.78	-0.86	2.29	0.512189 ±0.000015	-8.76	±0.30
115.5	12.91	0.71	2.96	-0.54	2.01	0.512180 ±0.000015	-8.94	±0.30
119.5	13.17	0.96	3.09	-	-	0.512161 ±0.000015	-9.31	±0.30
129.5	13.83	0.81	2.99	-	-	0.512156 ±0.000015	-9.41	±0.30
135.5	14.23	1.05	3.25	-1.16	1.98	0.512167 ±0.000015	-9.19	±0.30
135.5	14.23	-	-	-0.94	2.29	-	-	-
139.5	14.49	-	-	-0.96	2.51	0.512170 ±0.000015	-9.12	±0.30
159.5	15.88	0.91	3.45	-0.81	2.45	0.512153 ±0.000015	-9.47	±0.30
169.5	16.54	1.39	4.09	-0.76	3.47	-	-	-
179.5	17.20	1.53	4.30	-0.98	3.45	0.512170 ±0.000015	-9.12	±0.30
190	17.86	1.46	4.24	-1.10	3.70	0.512168 ±0.000015	-9.16	±0.30
198	18.39	1.65	4.39	-1.24	3.24	0.512153 ±0.000015	-9.46	±0.30
206	18.78	1.53	4.28	-0.90	3.53	-	-	-

Table 4